



Review

A Review of Carbon Nanotubes, Graphene and Nanodiamond Based Strain Sensor in Harsh Environments

Xiaoyan Wang^{1,2}, Eng Gee Lim^{1,2}, Kai Hoettges² and Pengfei Song^{1,2,*}

¹ School of Advanced Technology, Xi'an Jiaotong—Liverpool University, Suzhou 215123, China; xiaoyan.wang22@student.xjtlu.edu.cn (X.W.); enggee.lim@xjtlu.edu.cn (E.G.L.)

² Department of Electrical Engineering and Electronics, University of Liverpool, Liverpool L69 7ZX, UK; k.hoettges@liverpool.ac.uk

* Correspondence: pengfei.song@xjtlu.edu.cn; Tel.: +86-512-81889039

Abstract: Flexible and wearable electronics have attracted significant attention for their potential applications in wearable human health monitoring, care systems, and various industrial sectors. The exploration of wearable strain sensors in diverse application scenarios is a global issue, shaping the future of our intelligent community. However, current state-of-the-art strain sensors still encounter challenges, such as susceptibility to interference under humid conditions and vulnerability to chemical and mechanical fragility. Carbon materials offer a promising solution due to their unique advantages, including excellent electrical conductivity, intrinsic and structural flexibility, lightweight nature, high chemical and thermal stability, ease of chemical functionalization, and potential for mass production. Carbon-based materials, such as carbon nanotubes, graphene, and nanodiamond, have been introduced as strain sensors with mechanical and chemical robustness, as well as water repellency functionality. This review reviewed the ability of carbon nanotubes-, graphene-, and nanodiamond-based strain sensors to withstand extreme conditions, their sensitivity, durability, response time, and diverse applications, including strain/pressure sensors, temperature/humidity sensors, and power devices. The discussion highlights the promising features and potential advantages offered by these carbon materials in strain sensing applications. Additionally, this review outlines the existing challenges in the field and identifies future opportunities for further advancement and innovation.



Citation: Wang, X.; Lim, E.G.; Hoettges, K.; Song, P. A Review of Carbon Nanotubes, Graphene and Nanodiamond Based Strain Sensor in Harsh Environments. *C* **2023**, *9*, 108. <https://doi.org/10.3390/c9040108>

Academic Editors: Gil Gonçalves and Olena Okhay

Received: 12 September 2023
Revised: 3 November 2023
Accepted: 7 November 2023
Published: 14 November 2023



Copyright: © 2023 by the authors. Licensee MDPI, Basel, Switzerland. This article is an open access article distributed under the terms and conditions of the Creative Commons Attribution (CC BY) license (<https://creativecommons.org/licenses/by/4.0/>).

Keywords: carbon nanotubes; graphene; nanodiamond; strain sensor; harsh environment

1. Introduction

With the development of modern technology and the rapid rise of artificial intelligence technology, the research on various flexible devices has received widespread attention [1–5]. The types of strain sensors include pressure, torsional, tensile, and bending strain sensors, and the strain sensors can be divided into capacitance-type, piezoelectric-type, and resistance-type based on their working principles [6]. Among them, flexible strain sensors have attracted great interest from the industry and academia due to their promising applications in wearable devices [7,8], electronic skin [9,10], intelligent robots [11], healthcare monitoring [12], and human–machine interfaces [13,14]. As an important component in determining the performance of strain sensors, conductive materials generally include metallic materials (silver particles (AgNPs) [15,16], silver nano-wires (AgNWs) [16], gold nanowires (AuNWs) [17]), carbon-based materials (carbon black (CB) [18], carbon nanotubes (CNTs) [19,20], graphene [21,22] and nano diamond [23,24]), and intrinsically conducting polymers [25], etc. The combination of conductive materials with appropriate elastic polymer materials (silicone rubber [26], natural rubber (NR) [27], polyurethane (PU) [28]) can be fabricated strain sensors with high sensitivity and high stretchability.

The exploration of strain sensors with mechanical and chemical robustness, or functionality of water repellency enables the sensing coverage with a broader application

scenario to revolutionize our future. The importance of strain sensors in harsh environments cannot be overstated, as these sensors play a critical role in ensuring the safety, reliability, and performance of essential components and structures. In harsh environments, mechanical stress, extreme temperatures, and corrosive substances can lead to material fatigue and structural degradation. Strain sensors provide real-time data on the mechanical deformation and stress experienced by components, allowing for the early detection of potential failures. This timely information enables preventive measures to be taken, preventing catastrophic incidents and ensuring the safety of personnel and assets.

As technology continues to advance, strain sensors will play an increasingly vital role in various industries, such as aerospace, oil and gas, and civil engineering and health care. In space missions, deep-sea exploration, and mining operations, where human presence is limited or not feasible, strain sensors play a crucial role [29–32]. These sensors provide critical data on the structural integrity and performance of remote systems and equipment, ensuring the success and safety of these missions. By analyzing the strain data, engineers can assess the integrity of bridges, pipelines, aircraft, and other infrastructures. Moreover, strain sensors are employed in research and experiments conducted in extreme environments, such as high-temperature environments, high-pressure conditions, or corrosive atmospheres. They enable scientists to study materials and phenomena under these conditions, advancing our understanding of materials science and engineering. In industries with stringent safety regulations, such as nuclear power or aerospace, strain sensors are essential for compliance and certification. These sensors provide valuable data to ensure that components and structures meet safety standards and can withstand harsh conditions. In addition, as the population grows and the demand for healthcare increases, remote and personalized health monitoring gradually becomes the focus of attention, which can improve the accuracy of health diagnosis and also identify problems in time. Wearable strain sensors have been used extensively to monitor human physiological information, such as heartbeat, pulse, monitoring of respiratory and arterial signals, etc. [33,34].

In recent years, the advancement of materials science and nanotechnology has led to the development of cutting-edge sensing technologies that can withstand and operate in extreme environmental conditions [35–43]. Among these innovative sensors, strain sensors based on carbon materials have emerged as promising candidates for a wide range of applications in harsh environments [44–46]. Carbon-based strain sensors possess unique properties such as mechanical robustness, chemical stability, excellent electrical conductivity, and high sensitivity, making them ideal for monitoring structural integrity, deformation, and mechanical stress in extreme conditions [47–50].

The term “carbon materials” encompasses a diverse group of substances, including carbon nanotubes (CNTs), graphene, carbon black, and nanodiamonds, among others. These materials have been used in various aspects [51–53]. Each of these carbon-based materials has specific structural and electrical properties that can be harnessed to design strain sensors suitable for various harsh environments. Traditional strain sensors have been widely used [54–64]; however, their limitations in extreme conditions have driven the need for advanced sensing technologies. Carbon-based strain sensors offer several advantages over conventional sensors, including their ability to withstand harsh environments, high mechanical strength, and compatibility with diverse materials and substrates.

Previously, a few review articles for flexible strain sensors based on carbon materials have been reported [6,54,65–70], but most of them are only focused on the strain sensor used in normal environments. Here, we focus on strain sensors based on carbon nanotubes, graphene, and nanodiamond in harsh environments. Some typical strain sensors based on carbon nanotubes, graphene, and nanodiamond will be summarized in this review due to the unique property of these three kinds of carbon materials (Figure 1). This review will introduce the properties of carbon nanotubes, graphene, and nanodiamond (Table 1) and then show how the fabrication of carbon-based strain sensors withstand extreme conditions; their sensitivity, durability, and response time in Table 2. After that, the application was introduced in detail, including strain/pressure sensors, temperature/humidity sensors, and

power devices that are used in motion sensing, health monitors, electronic skin, and other applications (Figure 1). The discussion highlights the promising features and potential advantages offered by these carbon materials in strain sensing applications. This review will explore the advantages of carbon materials strain sensors in harsh environments, highlighting their unique characteristics and potential applications across various industries. From aerospace and automotive to healthcare and disaster rescue, these carbon-based strain sensors pave the way for enhanced safety, predictive maintenance, and performance optimization in the most demanding settings.

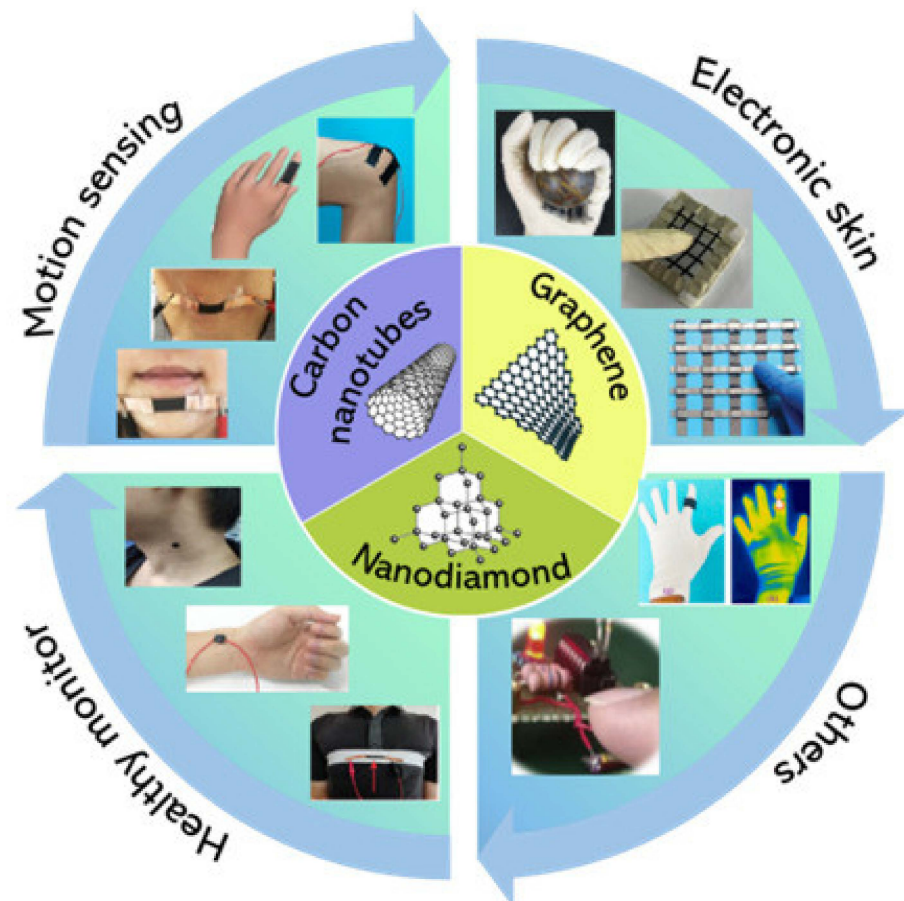


Figure 1. Application of strain sensors based on carbon nanotubes, graphene, and nanodiamond in harsh environments.

Table 1. The properties of carbon nanotubes, graphene, and nanodiamond.

Carbon Material	Electrical Conductivity	Thermal Conductivity	Young's Modulus	Crystal Lattice Parameters	Band Gap
CNT	$0.17\text{--}2.0 \times 10^7 \text{ S m}^{-1}$	$6600 \text{ W m}^{-1}\text{K}^{-1}$	270 to 950 GPa	sp^2 1.7 nm	~0.2 eV
Graphene	$224810^8 \text{ S m}^{-1}$	$5000 \text{ W m}^{-1}\text{K}^{-1}$	$853.3 \pm 0.9 \text{ GPa}$	sp^2 0.25 nm	1.25 eV
Nanodiamond	400 S m^{-1}	$2000 \text{ W m}^{-1}\text{K}^{-1}$	$880 \pm 90 \text{ GP}$	sp^3 2 to 3 nm	~5.5 eV

2. The Property of Carbon Nanotubes, Graphene and Nanodiamond

In harsh and demanding environments, the need for reliable and resilient sensors to monitor mechanical strain becomes paramount. Carbon materials, including carbon

nanotubes, graphene, and nanodiamonds, offer cutting-edge solutions as strain sensors in such challenging conditions. In Table 1, a comparison of the electrical conductivity, thermal conductivity, Young's modulus, crystal lattice parameters, and band gap of carbon nanotubes (CNTs), graphene, and nanodiamonds is listed [71–83]. Those carbon materials possess unique superiorities such as good electrical conductivity, high chemical and thermal stability, excellent mechanical property, low toxicity, as well as ease to be functionalized, endowing them with great potentiality for applications as strain sensors (Figure 1). These advanced carbon-based materials possess exceptional properties that enable them to withstand extreme temperatures, corrosive substances, and mechanical stress while accurately detecting and measuring strain.

Carbon nanotubes are one-dimensional nanomaterials with exceptional electrical conductivity and mechanical strength [73]. There are two classes of CNTs, single-walled carbon nanotubes (SWCNTs) and multiwalled carbon nanotubes (MWCNTs). Carbon nanotubes, tubular structures composed of rolled-up graphene sheets, are renowned for their exceptional mechanical strength. This property empowers them to endure high levels of mechanical stress in harsh environments without deformation or failure. Additionally, carbon nanotubes exhibit high sensitivity to mechanical strain, detecting even minute deformations with high accuracy. This is because carbon nanotubes have an exceptionally high aspect ratio, with lengths up to micrometers and diameters at the nanoscale, allowing for efficient load transfer and strain distribution within the material, enhancing their sensitivity to mechanical deformations even in harsh environments. Furthermore, the lightweight and small size of carbon nanotubes allow for seamless integration into various structures without compromising overall mass. By capitalizing on their electrical conductivity ($0.17\text{--}2.0 \times 10^7 \text{ S m}^{-1}$), carbon nanotubes serve as piezoresistive sensors, directly measuring electrical resistance changes in response to mechanical strain, thus ensuring precise and real-time strain monitoring. The nanoscale dimensions of carbon nanotubes make them suitable for sensing strain at small scales, such as in microelectromechanical systems (MEMS) or nanodevices, enabling applications in miniaturized and complex systems. Importantly, they have good chemical stability. Their chemical inertness shields them from corrosion and degradation when exposed to aggressive chemicals or harsh substances.

Graphene, a single layer of carbon atoms arranged in a two-dimensional honeycomb lattice, possesses extraordinary mechanical strength and superior electronic property [84]. Graphene, graphene oxide (GO), and reduced graphene oxide (RGO) have attracted much attention because of easy operation and high yields of bulk-quantity and they have been demonstrated for usages of strain sensors [85]. Graphene's atomic thickness ensures minimal interference with the mechanical properties of the host material, making it suitable for surface-mounted and embedded sensing. This intrinsic sensitivity to mechanical strain enables graphene to detect and measure even the most subtle deformations with precision. Graphene's exceptional mechanical strength, combined with its high electrical conductivity (10^8 S m^{-1}), results in superior sensitivity and fast response times when used as a piezoresistive strain sensor. These attributes are crucial for real-time monitoring of dynamic events and rapid mechanical changes in harsh environments. Similar to carbon nanotubes, graphene is chemically inert, resistant to corrosion, and stable in the presence of harsh substances. Its thermal stability allows it to operate effectively across a broad range of temperatures, making it an ideal candidate for applications in extreme thermal environments. Graphene can be synthesized in various forms, such as flakes, films, or as part of composites, allowing for versatile strain sensor designs catering to specific application requirements [86].

Nanodiamonds, nanometer-sized diamond particles composed of carbon atoms in a diamond crystal lattice, boast extreme hardness and durability. This exceptional mechanical strength renders them highly resistant to wear and damage in harsh environments. Like carbon nanotubes and graphene, nanodiamond (ND) is from a family of carbon materials with unique properties including extreme hardness, low friction coefficient, high corrosion resistance, high thermal conductivity, along with excellent mechanical and chemical stabil-

ity. The extreme hardness of nanodiamonds (Young's modulus 880 ± 90 GP) makes them resistant to wear and degradation, allowing for long-term and reliable strain monitoring, even in abrasive environments. ND also has a large surface area and possesses a versatile surface chemistry that can be tailored for each application via surface termination and functionalization [87,88]. Synthetic diamond, due to its chemical inertness and resistance, has the potential to be a perfect passivating material [89]. It is very cost-effective because of its production at bulk quantity using a detonation method [90,91]. Nanodiamonds demonstrate chemical inertness, preserving their stability and integrity in the face of corrosive substances. Furthermore, nanodiamonds can withstand high temperatures, making them well-suited for applications in harsh thermal environments. Their small size and surface functionalization capabilities offer the flexibility to tailor their properties for specific strain sensing applications. Nanodiamonds have excellent biocompatibility, making them suitable for strain sensing applications in biological or medical environments, including monitoring the mechanical strain of tissues or implants. Nanodiamonds can also serve as strain sensors based on stress-induced changes in their optical properties, providing an alternative sensing mechanism.

3. Fabrication Methods and Performance of Strain Sensor on Extreme Conditions

3.1. Fabrication Method of Strain Sensor on Extreme Condition

Creating a carbon-based strain sensor for harsh environments involves designing a robust and durable device capable of measuring mechanical stress or strain while withstanding extreme conditions. Various manufacturing techniques, such as coating, 3D printing, chemical vapor deposition, transfer, and spinning methods, are utilized in the production of carbon materials strain sensors. Coating technology is widely applied to manufacture thin film and fabric sensors, while 3D printing is employed for pattern generation [92]. Chemical vapor deposition is primarily used for carbon nanotubes growth. Additionally, the grown carbon materials can be transferred using a flexible substrate combined with a transfer method [93]. The integration of spinning [94] and coating processes enables the fabrication of high-performance fiber optic strain sensors. Furthermore, other methods like layer-by-layer (LBL) assembly technology, photolithography, and solution mixing [95] are also employed to manufacture flexible strain sensors. The fabrication methods of carbon nanotubes-, graphene-, and nanodiamond-based strain sensors reviewed are listed in Table 2.

3.1.1. Fabrication of Carbon Nanotubes Strain Sensors

Several synthesis methods have been reported to incorporate CNTs into various polymeric matrices, aiming to prevent CNT agglomeration and achieve uniform dispersion within the polymer matrix. However, there is no one-size-fits-all approach to attain perfect dispersion of different CNTs in various types of polymer matrices. The selection of an appropriate dispersion technique depends on several factors, including the physical state of the polymer (solid or liquid), the chemical nature (thermoplastic or thermoset), the dimensions and content of the introduced CNTs, the availability of fabrication processes and techniques, ease of synthesis from suitable monomers, desired performance characteristics of the composites, cost constraints, and the choice of solvent parameters. Li et al. [96] and Zhang et al. [97] chose the one-pot method to fabricate the CNT strain sensor. Under UV light, the reaction occurred very rapidly and efficiently within a few minutes, showing fast and pollution-free characteristics [97]. In another method, the PVA was dissolved by heating in the water/glycerol(Gly) binary solvent, and the hydrogels were formed after several freeze-thaw cycles, with the hydrogen-bonded microcrystalline region acting as the crosslinking point [96]. A facile spraying method was used to prepare superhydrophobic and conductive coatings on elastic tape with a hierarchical fluorinated carbon nanotubes (FCNT)/SiO₂ nanoparticle structure in Figure 2a [98]. The flexible and super-hydrophobic elastic tape covered with FCNT/SiO₂ was successfully prepared (Figure 2b), and the hierarchical FCNT/nanoparticle structure can be observed in Figure 2c.

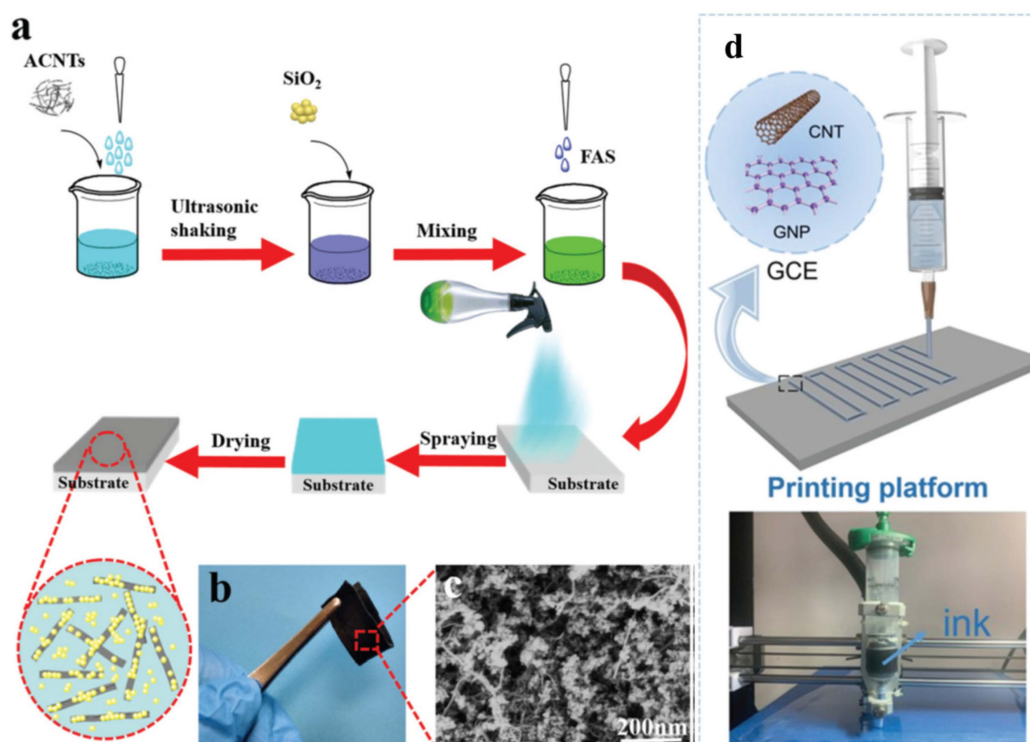


Figure 2. (a) Schematic diagram for the preparation of FCNT/SiO₂ coating on elastic tape. (b) Photograph of one piece of superhydrophobic and conductive elastic tape displaying excellent flexibility. (c) SEM image of the FCNT/SiO₂ coating [98]. (d) Schematic illustration of the direct ink writing (DIW) process of GCE fibers [99].

3.1.2. Fabrication of Graphene Strain Sensors

The development of advanced fabrication approaches for graphene-based strain sensors is in its early stages, with future progress in this direction being crucial. One of the primary goals is achieving highly efficient manufacturing of flexible sensors. Traditional fabrication methods often suffer from high processing costs and complex manufacturing processes, necessitating research into scalable, customizable, and environmentally friendly fabrication techniques suitable for large-scale production. Additive manufacturing and printing technologies show promise in this regard, enabling the creation of intricate 3D structures that expand the potential applications of these sensors. Another essential aspect is ensuring the production of sensors with high repeatability. When these sensors are used as arrays, variations among different sensors can be significant, requiring individual calibration and more complex circuitry. As the number of sensors increases, the tolerance for inter-sensor variability decreases significantly, posing challenges to the sensing operation. In composite strain sensors, inter-sensor variability often arises from the aggregation and uneven dispersion of conductive materials within the elastomeric matrix, especially when the sensor size is reduced. To ensure the reproducibility of fabrication processes, adopting a coupled printing technique may prove beneficial, enabling large-scale production of strain sensors with improved uniformity and reliability. Many researchers used a coating method to prepare graphene-based strain sensors in extreme situations [45,100–102]. Moreover, direct ink writing (DIW) is also a facile way. Zhu et al. developed a DIW assembly approach for fabricating fiber-shaped strain sensors by incorporating graphene nanoplatelet (GNP)/carbon nanotube (CNT) hybrid fillers into the silicone elastomer, as shown in Figure 2d [99].

3.1.3. Fabrication of Nanodiamonds Strain Sensors

Nanodiamonds are typically synthesized through various methods, such as detonation, chemical vapor deposition (CVD) [89,103], or high-pressure high-temperature (HPHT) processes. Detonation synthesis involves detonating explosives in a controlled environment to

create high-pressure and high-temperature conditions, leading to the formation of nanodiamonds. CVD involves introducing carbon-containing gases into a reactor at high temperatures to deposit nanodiamonds on a substrate. HPHT utilizes extreme pressure and temperature to convert carbon sources into diamond structures. After synthesis, nanodiamonds may require purification to remove impurities and unwanted by-products. Functionalization can be performed to modify the surface properties of nanodiamonds, enhancing their dispersion and compatibility with the substrate and sensor materials. Choose a suitable substrate material based on the application requirements, such as flexibility, rigidity, and compatibility with nanodiamonds and other sensor components. Common substrates include silicon, glass, flexible polymers, or even textile materials. Nanodiamonds can be deposited on the substrate using techniques like spin coating, dip coating, or inkjet printing. In coating [104], a solution containing nanodiamonds is dispensed onto the substrate and then spun to achieve a uniform coating. In inkjet printing [105], nanodiamonds are dispersed in a liquid solution and printed onto the substrate in a controlled pattern. A flower-like molybdenum disulfide (MoS_2)/nanodiamond (ND) nanocomposite was successfully prepared via an easy hydrothermal synthesis method and fabricated into humidity sensors in Figure 3 [106].

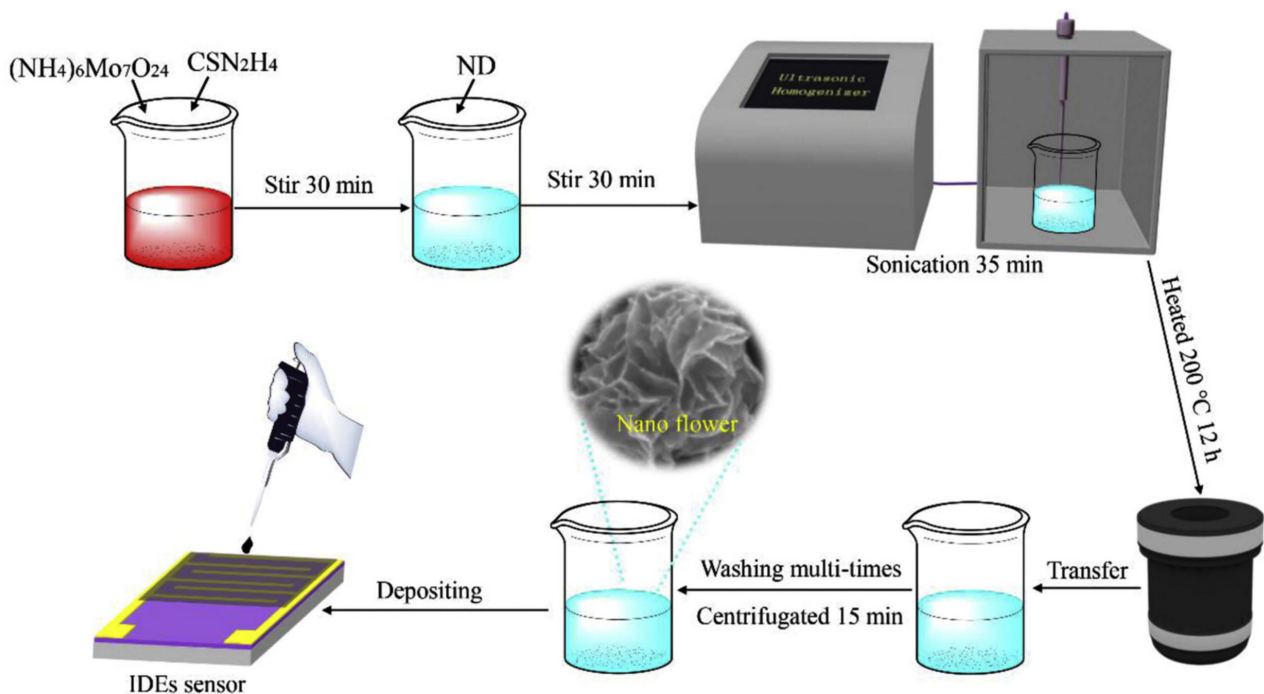


Figure 3. Fabrication route of MoS_2/ND nanocomposite via an easy hydrothermal synthesis method [106].

3.2. Performance of Strain Sensors in Harsh Environment

3.2.1. Ability to Resist Harsh Environment

Strain sensors based on carbon materials possess unique properties that allow them to resist and perform well in harsh environments. These sensors exhibit mechanical robustness, chemical stability, high thermal resistance, and excellent electrical conductivity, making them suitable for monitoring strain in extreme conditions. Carbon materials, such as carbon nanotubes and graphene, are known for their exceptional mechanical strength and toughness. They can withstand high mechanical stress, including tension, compression, and bending, without undergoing significant deformation or failure. This mechanical robustness enables strain sensors to operate reliably in environments with intense mechanical forces, such as aerospace applications, heavy machinery, or offshore structures. The strain sensors used in harsh environments have been summarized in Table 2.

Chemical Stability: Many carbon-based materials, including carbon nanotubes, graphene, and nanodiamond, exhibit outstanding chemical stability. They are resistant to corrosion,

oxidation, and chemical reactions, even when exposed to aggressive substances or harsh chemicals. This chemical stability ensures that strain sensors remain functional and accurate in chemically harsh environments, such as chemical processing plants or oil and gas facilities. Especially, Ding and Zhu reported that the strain sensors can resist the strong acid and strong alkaline, pH 2–13 [107] and pH 1–14 [108].

Environment Stability: The sensor's sensitivity can also be affected by environmental factors such as temperature and humidity. Stability under different conditions is essential for accurate strain measurements. Carbon materials are known for their high thermal stability, enabling strain sensors to maintain their structural integrity and electrical conductivity at high and low temperatures and high humidity. Unlike some conventional materials, carbon-based strain sensors do not become brittle or lose their electrical properties under extreme hot or cold conditions. Carbon materials possess excellent thermal conductivity and high thermal stability. Strain sensors based on carbon materials can operate effectively at elevated temperatures, withstanding extreme heat and thermal fluctuations. This thermal resistance is crucial in applications where sensors need to monitor strain in high-temperature environments, such as aerospace propulsion systems or industrial furnaces. Carbon materials generally exhibit low thermal expansion coefficients, meaning they experience minimal dimensional changes in response to temperature variations. This characteristic ensures that strain sensors based on carbon materials can accurately detect mechanical deformations without significant interference from temperature-induced strain. The inherent electrical conductivity of carbon materials, such as carbon nanotubes, graphene, and nanodiamond remains intact at low temperatures. This property allows strain sensors to maintain their piezoresistive effect even in cold environments, ensuring reliable and sensitive strain measurements. Carbon nanotubes-based strain sensors are stable even at high temperatures, 316 °C [109], or at ultralow temperatures, −196 °C [94], and even work under water [99]. For example, a piezoresistive sensor based on nanodiamond proved that the working temperature is 25 °C up to 300 °C [89].

3.2.2. Sensitivity

The sensitivity of a carbon-based strain sensor refers to its ability to detect and respond to small changes in mechanical strain. In other words, it measures how effectively the sensor can convert mechanical deformation into an electrical signal. Sensitivity is a critical parameter for strain sensors as it determines the level of accuracy and precision in measuring strain.

Gauge Factor

The sensitivity of a strain sensor is characterized by the gauge factor (GF), and the GF of a resistive-type strain sensor is expressed as Equation (1).

$$GF = \frac{(\Delta R/R_0)/R_0}{\epsilon} = \frac{[(R - R_0)/R_0]/R_0}{\epsilon} \quad (1)$$

where R is the actual measured resistance value during sensor deformation, R_0 is the initial resistance value of the sensor, and ϵ is the strain value that occurs when the sensor is subjected to an external force. The higher GF values indicate that the sensor is more sensitive to the applied strain. The GF values of different CNT-, graphene-, and nanodiamond-based strain sensors in harsh environments are listed in Table 2.

Piezoresistive Effect

The piezoresistive effect is a phenomenon observed in certain materials where their electrical resistance changes in response to applied mechanical stress or strain. In other words, the electrical conductivity of the material is influenced by mechanical deformation. The term “piezoresistive” is derived from “piezo”, meaning pressure or stress, and “resistive”, referring to electrical resistance. Piezoresistive materials are widely used in the construction of strain sensors and pressure sensors. When these materials are subjected

to mechanical stress or strain, their atomic arrangement undergoes changes that alter the movement of charge carriers, such as electrons, within the material. As a result, the electrical resistance of the material changes proportionally to the applied stress [110].

There are two main types of piezoresistive effects:

Positive Piezoresistive Effect: In materials exhibiting a positive piezoresistive effect, the electrical resistance increases with increasing applied stress. This means that as the material undergoes compression or tension, its resistance to the flow of electric current increases.

Negative Piezoresistive Effect: In materials showing a negative piezoresistive effect, the electrical resistance decreases with increasing applied stress. In this case, the material becomes more conductive under mechanical deformation.

The piezoelectric charge coefficient (d) is a material property that relates the electric charge (Q) generated in a material to the applied mechanical stress (σ) or strain (ϵ). It is a measure of a material's ability to convert mechanical energy into electrical energy and vice versa. The calculation of the piezoelectric charge coefficient depends on the specific measurement setup and units used.

In the direct piezoelectric effect, an applied mechanical stress or strain generates an electric charge in the material, while in the converse piezoelectric effect, an applied electric field induces mechanical strain or stress. The piezoelectric charge coefficient is typically given in units of picocoulombs per newton (pC/N) or coulombs per newton (C/N).

The general formula to calculate the piezoelectric charge coefficient (d) is expressed as Equation (2):

$$d = \frac{Q}{F} \quad (2)$$

d is the piezoelectric charge coefficient (C/N or pC/N)

Q is the electric charge generated (in coulombs, C, or picocoulombs, pC)

F is the applied force (in newtons, N)

Piezoresistive materials commonly used in strain sensors include silicon and carbon-based materials. These materials are carefully integrated into the sensor's design to measure mechanical strain or pressure accurately and convert it into a corresponding electrical signal. The piezoresistive effect allows for the creation of highly sensitive and responsive sensors, making them valuable in various applications, including structural monitoring, medical devices, robotics, and automotive systems. Piezoelectric charge coefficient of a CNT-based strain sensor is 9.4 pC/N [95].

In some research, different definitions to assess the sensitivity of the strain sensor have been used.

- The sensitivity of the strain sensor is expressed as Equation (3) [94].

$$S = \frac{\Delta I}{I_0} \quad (3)$$

The relative current change ($\Delta I/I_0$) under a changing tensile load. Here, ΔI defines the current difference between the loaded and unloaded fiber and I_0 is the original current.

- The sensitivity of the composite sensor is expressed as Equation (4) [97].

$$S = \Delta I/I_0 P (\Delta R/R_0 P) \quad (4)$$

where P is the applied pressure, the relative resistance ΔI (ΔR) is defined as $|I(R) - I_0(R_0)|$, where $I_0(R_0)$ is the initial electric current (resistance) and $I(R)$ represents the real-time electric current (resistances) under various deformations.

- The sensitivity of the pressure sensor (S) is defined as Equation (5) [111].

$$S = (\Delta R/R_0)/\Delta P \quad (5)$$

as the derivation of the resistance change rate ($\Delta R/R_0$) with pressure.

- The sensor sensitivity (S) is calculated by Equation (6) [106].

$$S = (C_X - C_{11}) / (RH_x - RH_{11}), \quad (6)$$

where C_{11} is the sensor capacitance at 11% RH, and C_X represents the capacitance of the sensor in the $x\%$ values.

3.2.3. Response and Recovery Time

The response and recovery time of a strain sensor refer to the time it takes for the sensor to detect and register a change in mechanical strain (response time) and the time it takes for the sensor to return to its original state after the strain is removed (recovery time).

The response time of strain sensors is relatively fast, typically in the millisecond to microsecond range, depending on the specific sensor and its application. It is proved that a strain sensor based on rGO has very fast response time, only 22 ms [102]. Most of response time of the strain sensors that we reviewed in this review are all less than 1 s detailed in Table 2. The recovery time may also be relatively quick, but it can vary depending on the material properties and the sensor's design.

It is important to note that the actual response and recovery times for a strain sensor will depend on the specific sensor's characteristics, the materials used, and the intended application. Manufacturers and researchers continuously work to improve the speed and accuracy of strain sensors for various industries and applications, including structural health monitoring, robotics, aerospace, and wearable devices.

3.2.4. Durability

Dynamic durability is the ability of a strain sensor to maintain stable electrical conductivity after a certain cycle or over time. Ideally, the sensor should ensure that the resistance value does not change during the continuous stretch and release cycle. At the same time, the sensor will be able to perform a longer cycle test to ensure that it has a longer service life. To perform durability testing, the sensor is cyclically stretched and released at a certain strain value. Most of the sensors prepared based on CNTs/graphene/nanodiamond in harsh environments reported so far can achieve more than 1000 stretch release cycle tests, as shown in Table 2. The fiber-based sensors can provide better tensile performance while providing excellent dynamic durability of the sensor. A graphene/CNT/silicone composite strain sensor response of the strain sensor possesses excellent stability and durability without an apparent change in the resistance signal, fully proving its stable and repeated recoverability during the 10,000 stretching/releasing cycles [99].

Ensuring reliable and enduring performance, the durability of strain sensors in harsh environments is a paramount concern. Such environments encompass extreme temperatures, corrosive chemicals, high mechanical stress, radiation exposure, or a combination of these factors, presenting formidable challenges to strain sensors. Key factors influencing their durability include material selection, favoring robust and resilient options like carbon nanotubes, graphene, nanodiamonds, ceramics, and piezoelectric materials. To shield sensitive components from the environment, proper encapsulation and packaging techniques are employed, incorporating hermetic sealing and protective coatings. Mechanical durability is addressed through sensor designs tailored to withstand high mechanical stress, shocks, and vibrations, crucial when sensors are integrated into moving or vibrating structures. Washing procedure has a direct impact on electrical conductivity and abrasion resistance is one of the factors that affects the life and wear performance of the fabric. Rehman et al. [104] found that the fabric coated with PANI-ND (polyaniline-nanodiamond) improved significantly along with durability against washing and abrasion, without affecting its breathability. These PANI-ND nanocomposites are still present on the surface of the fabric even after five commercial washing cycles using 20 mL/g liquor-to-fabric ratio at 40 °C for 30 min along with 25 steel balls. Moreover, this nanocomposite helped to resist the degradation of pristine wool fibers during 20,000 abrasion cycles.

Table 2. Summary of fabrication methods and performance of strain sensors in this review.

Carbon Material	Fabrication Method	Property	Sensitivity (GF/S)*	Response Speed	Durability	Ref.
MWCNT	unidirectional freeze-drying method	25, 177, and 316 °C	1.23	stable	high-strain cyclic compression	[109]
SWCNT	one-pot method	−70 to 25 °C	3.76	—	1600 cycles	[96]
MWCNT	a one-pot radical polymerization process	−20 to 80 °C	1.77 at 25 °C	—	capacitance almost the same (1000 cycles)	[36]
Graphene	free radical polymerization	−20 to 70 °C	—	—	88.2% of capacitance retention (6000 cycles)	[112]
CNT	solution mixing	60% RH condition	piezoelectric charge coefficient 9.4 pC/N	—	—	[95]
CNT	freeze drying and thermal imidization technique	250 °C	1.4	response time 50 ms/recovery time 70 ms	1000 cycles	[113]
rGO	the conformal coating	−40 °C/25 °C and 50% RH for 20 days	Pulse rate of 75 beats/min	0.1 s	2000 times (2 kPa)	[45]
CNT	wet spinning method	−196 to 100 °C	S = 0.12	—	long life (1000 cycles)	[94]
MWCNT/RGO	dip-coating	−30 and 80 °C	—	—	1000 cycles	[100]
CNT	a convenient solvent replacement strategy	−60 to 60 °C	8.5	200 ms	30 days in normal environment	[114]
rGO/CNT	vacuum filtration process	−40 °C to 200 °C	—	—	90% capacitance (105 cycles)	[115]
Graphene/CNT	DIW	humidity/water exposure	14550.2 (100%)	170 ms	10,000 cycles	[99]
CNT	vacuum-assisted formation of thin CNT networks	RH 35–55%/water exposure	6–10	—	—	[116]
CNT	one-pot	25–70 °C	S = 20.3	—	compressive strain (0.1–70%) and loading weight (55–150 g)	[97]
rGO	chemical reduction, thermal reduction	−60 °C	—	—	87.5% capacitance (5000 charge/discharge cycles at −20 °C)	[117]
CNT	CNT suspension was mixed with Ti ₃ C ₂ T _x suspension	−20 to 80 °C	13.3 (60.3%)	—	1000 cycles	[118]

Table 2. Cont.

Carbon Material	Fabrication Method	Property	Sensitivity (GF/S)*	Response Speed	Durability	Ref.
CNT	a direct pyrolysis process	−196 °C	1.65	—	5000 cycles (40%)	[119]
CNT	the film transfer approach	water	2.4	—	—	[93]
CNT	drying mixing method	hot-humidity/−40 to +50 °C	high sensitivity	—	150 cycles (50%)	[120]
SWCNT	dip coating of SWCNTs/chemical polymerization	144.6 °C	9.57	—	500 cycles (20%)	[121]
FCNT	a facile spraying method	moisture, acidic, and other harsh environments	1800	—	—	[98]
CNTs/rGO	coating	water	685.3 (482%)	response/recovery 200 ms	1000 cycles	[92]
MWCNT	spray coating	water, pH 13/2	69.84 (65–80%),	60–80 ms	over 1000 cycles	[107]
CNTs/graphene	freezing-drying	160 °C	high sensitivity (0.25 kPa ^{−1})	120 ms	>800 cycles	[111]
graphene–CNT	thin film using a bar-coating technique	−150 °C to + 150 °C	118	—	5000 cycles	[101]
GO/RGO	pad dyeing	22.8 °C to 47.3 °C RH 39–71%	2.79 (0–50%)	<60 ms	3000 cycles (10%)	[122]
graphene	one-pot solution-casting process	pH 1–14/humidity	173.17 (100%)	—	2000 cycles (50%)	[108]
rGO	dip-coating	humid, sweaty, underwater, −40 °C	−2.08 (0–60%)	22 ms	4000 cycles	[102]
Nanodiamond	coating/in situ polymerization technique	40 °C for 30 min along with 25 steel balls	1.4 (40–100%)	—	washing/rubbing	[104]
Nanodiamond	hydrothermal synthesized method	11–97% RH	S = 3500, relative humidity 100%	response < 1 s/recovery time~0.9 s	stable one month	[106]
Nanodiamond	vacuum-assisted filtration	100.4 °C	thermal conductivity of 17.43 W/m·K	—	—	[123]

Table 2. Cont.

Carbon Material	Fabrication Method	Property	Sensitivity (GF/S)*	Response Speed	Durability	Ref.
Nanodiamond	self-assessable	thermal stability	thermal conductivity of 30.99 and 6.34 W/m·K	—	1000 cycles	[124]
Ultrananocrystalline diamond	hot filament chemical vapor deposition (HFCVD) and photolithographic and etching processes	25 °C–300 °C	9.54 ± 0.32	—	—	[89]
Nanodiamond	inkjet printing locally	against harsh media	diamond layer does not hamper the stability of the device	—	—	[105]
Nanodiamond	a directed patterned growth of NCD film by microwave plasma-enhanced chemical vapour deposition (CVD)	200 °C	8 ± 0.5	—	—	[103]

4. Carbon Materials Based Strain Sensor on Extreme Temperature Condition

The operating temperature of the strain sensors is crucial to their wide applicability. Some strain sensors are often used at room temperature, but their performance may deteriorate at low and/or high temperatures. Therefore, it is crucial to develop strain sensors that can be used at low and/or high temperatures to expand their range of use.

4.1. CNT-Based Strain Sensor on Extreme Temperature Condition

Anisotropic composite polyimide aerogels (CPIAs) were prepared via the unidirectional freeze-drying method using PI (Polyimide) as the polymer matrix and MWCNTs as the filler [109]. The obtained CPIAs exhibited low density, high porosity, good mechanical behavior, and stable electrical responsiveness across a wide temperature range (from 25 to 316 °C). As a strain sensor, the CPIA also works effectively as a lightweight sensitive strain sensor gauge factor (GF) of 1.23 and stability cyclic testing over 1000 cycles. Due to the good thermal stability of the CPIAs, under high temperature conditions, the CPIAs' responsiveness remained stable, as did their gauge factor values, which were not significantly affected by temperature. There is also other research about strain sensors on high temperature environment. The polypyrrole (PPy)/single-walled carbon nanotube (SWCNT)/polydopamine(PDA)/cotton composite fabric reach showed outstanding heating performance at 144.6 °C [121]. A polyimide (PI)/carbon nanotubes (CNT) composite aerogel with the merits of super elasticity, high porosity, robustness, and high-temperature resistance was successfully prepared, and can be stable even at 250 °C [113]. Li et al. [96] reported a conductive hydrogel consisting of a glycerol (Gly)-water binary solvent and added tannic acid (TA)-coated carboxymethylated cellulose nanofibrils (CMCNFs) to poly (vinyl alcohol) (PVA) as a functional filler to improve the hydrogel's mechanical properties. This frost-resistant strain sensor showed strain sensitivity (GF of 3.76), and cyclic stability (1600 cycles). The differential scanning calorimetry (DSC) curves of the hydrogel with different Gly contents are horizontal straight lines in the temperature range of -70 to 25 °C, indicating that no phase transition occurred in the Gly/water binary solvent system during the heating process in this range. In addition, Huang et al. [94] reported light weight porous aramid nanofibers (ANF) and carbon nanotubes (CNT) aerogel fibers coated with polypyrrole (PPy) layers prepared with low density (56.3 mg/cm³), conductivity (6.43 S/m), and tensile strength (2.88 MPa), which were used as motion sensors with high sensitivity (0.12) and long life (1000 cycles). They also showed excellent mechanical strength and flexibility, a strong bending property at low temperatures, -196 °C, and high-temperature resistance at 100 °C, which is mainly due to the good network structure of the ANF aerogel. An environment tolerant conductive hydrogel based on nanocomposite polyacrylamide/montmorillonite/carbon nanotube (MMCOHs) was prepared by a convenient solvent replacement strategy, featuring remarkable mechanical properties, anti-freezing ability (-60 °C), long-term environmental stability (>30 days), and anti-drying behavior (60 °C), simultaneously [114]. MMCOH displayed excellent flexibility to twist at will and could be easily bent at -60 °C, as shown in Figure 4a, and had stretchability and conductivity at -60 °C, as shown in Figure 4b,c. The sensor based on MMCOH displays an extremely wide sensing range (0-4196%), high sensitivity (GF = 8.5), rapid response time (200 ms), and excellent durability, benefiting from the inherent stretchability and stability of the organohydrogel. The MMCOH was obtained after directly immersing polyacrylamide/montmorillonite/carbon nanotube hydrogels (MMCH) into a glycerol solution through a solvent-replacement strategy. Other strain sensors based on CNT are well developed and the temperature resistance is varied (20~80 °C [36,118], 25~70 °C [97], and -40~50 °C [120]), and in the evening reaching a temperature of -196 °C [119]).

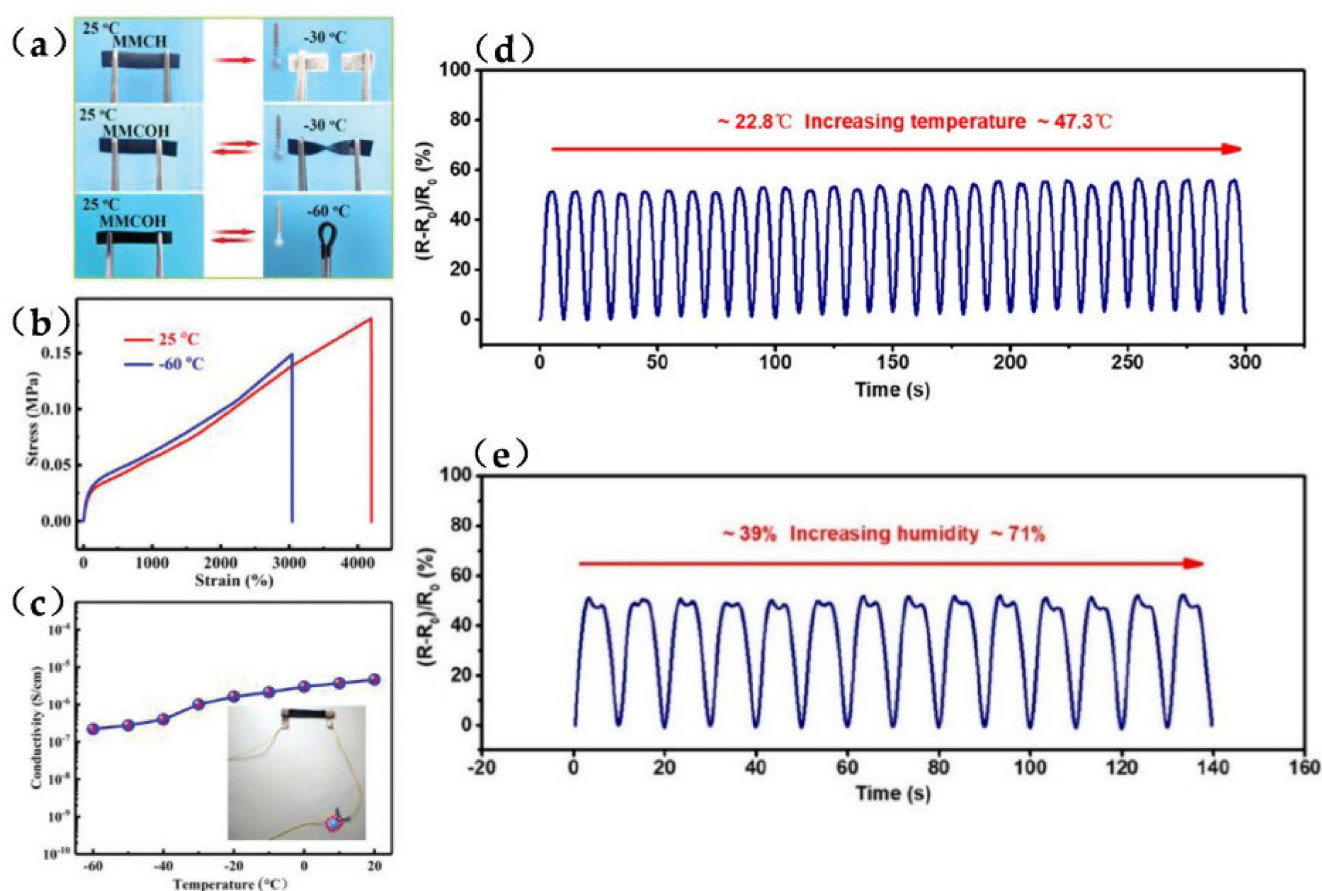


Figure 4. The environmental tolerance of the MMCOH. (a) Photographs of the anti-freezing behavior of MMCH and MMCOH. (b) Stress–strain curves of MMCOH at 25 and -60 °C. (c) Conductivity of MMCOH from -60 to 20 °C [114]. (d) Electrical signals of the sensor under a cyclic strain of 15% at temperatures from ≈ 22.8 °C (room temperature) to ≈ 47.3 °C, presenting stability of the sensor at different temperatures. (e) Electrical outputs of the GMF sensor with a recurrent strain of 15% in the process of humidity changing from ≈ 39 to ≈ 71 %, presenting stability of the sensor in different humidities [122].

4.2. Graphene Based Strain Sensor on Extreme Temperature Condition

A highly breathable graphene-modified fabric (GMF) strain sensor with an insensitive response to changes in temperature and humidity within a certain range was developed, which possesses sensing independence against temperature from 22.8 to 47.3 °C and relative humidity ranges of 39% to 71%. Figure 4d [122] displays the electrical response of the GMF sensor under a cyclic strain of 15% in changeable temperature. The signals maintain stability with highly reproducible signaling patterns when the temperature increases from 22.8 to 47.3 °C. The insensitivity of the GMFs sensor to temperature change is attributed to the rGO on the *Calotropis gigantea* yarn (CGY) surface exhibiting a decrease in the hopping charge transport number and the slight thermal generation of fewer carriers. The electrical signals of the sensor were measured under a recurrent strain of 15%, and the results indicate that the electrical response remains highly steady and repeatable during the humidity change process (Figure 4e). Moreover, the nanocomposite organohydrogel is prepared from the conformal coating of functionalized rGO network by the hydrogel polymer networks consisting of PVA, phenylboronic acid grafted alginate (Alg-PBA), and polyacrylamide (PAM) in the binary ethylene glycol (EG)/H₂O solvent system (Figure 5a) [45]. The nanocomposite organohydrogel exhibits reliable anti-freezing properties (-40 °C) and self-healing properties without any other external stimuli, and can be stably stored for 20 days (Figure 5b,c). Deng et al. [112] reported that a N-doped

hydrogel electrode showed excellent temperature stability in the range of -20 to 70 °C and a stretchability that reached 950%. A low-temperature-resistant organohydrogel electrolyte could be stretched up to 400% strain and still maintain stable mechanical properties up to -60 °C, combining the rGO electrodes with the organohydrogel electrolyte [117]. GO/RGO can be mixed with other carbon materials to form strain sensors that can be stable at low and high temperatures [99–101,115]. Li et al. reported a high performance textile-based stretchable supercapacitor stable over a wide temperature range, from -30 to 80 °C [100]. In this study, a multiwalled carbon nanotubes (MWCNT)/reduced graphene oxide (RGO) nanocomposite was used to fabricate a stretchable electrode. These carbon-based electrode materials are expected to be stable over a wide range of temperatures because the energy storage mechanism of electrical double-layer capacitors relies only on the electrostatic adsorption and desorption of electrolyte ions onto the electrode surface [29,40]. Furthermore, the encapsulated supercapacitors retain the capacitance during being immersed in water for a few days. Similarly, a flexible serpentine-structured graphene–CNT paper strain sensor in variable temperature environments was tested using a cryogenic and hot setup and the device showed robust performances, from -150 °C to 150 °C, which also demonstrated a high sensitivity with a GF of 118 [101]. A flexible rGO/CNT hybrid film can operate at extreme temperatures (down to -40 °C and up to 200 °C) with excellent electrochemical property and high durability [115].

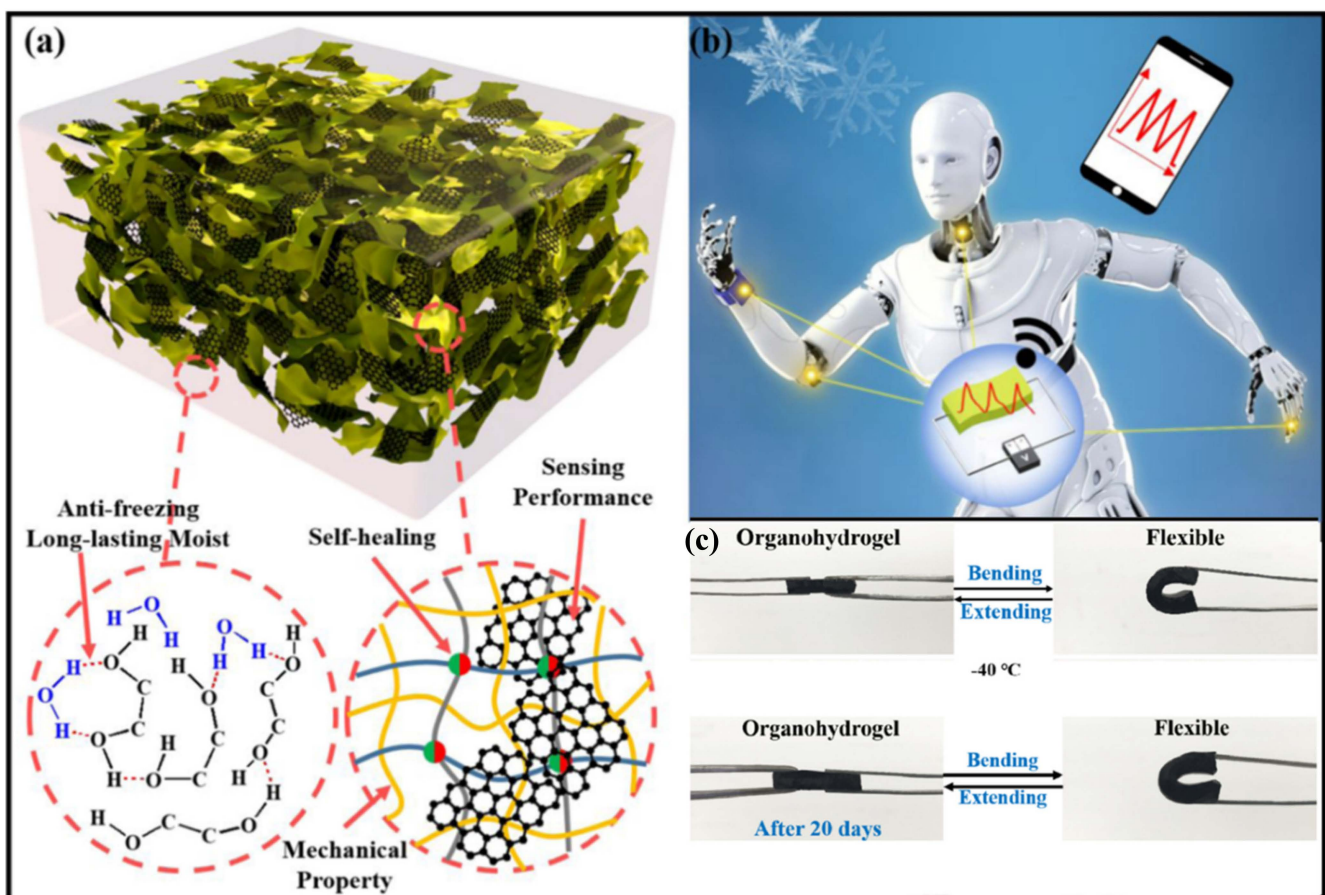


Figure 5. (a) Acrylamide (AM), Alg-PBA, and PVA were sequentially added to the rGO-containing EG/H₂O solution, and the polymerization was carried out to obtain PAM network and the conductive nanocomposite organohydrogel. (b) Conductive nanocomposite organohydrogel could be assembled as human-motion sensors with low temperature tolerance (-40 to 0 °C) for accurate detection of both tiny (swallowing and pulse) and large (finger bending and elbow bending) human activities. (c) Organohydrogels were bent after cooling at -40 °C and after 20 days of storage at 25 °C and 50% humidity, the organohydrogels maintained excellent elasticity [45].

4.3. Nanodiamonds Based Strain Sensor on Extreme Temperature Condition

A piezoresistive sensor prototype based on n-type conductive ultrananocrystalline diamond (UNCD) was developed. The respective piezoresistive response of such films was analyzed and the gauge factor was evaluated in both transverse and longitudinal arrangements, also as a function of temperature from 25 °C up to 300 °C [89]. Another piezoresistive sensor was produced. The gauge factor of boron-doped nanocrystalline diamond (NCD) films was around 8, and in the range from room temperature up to 200 °C, the sensor was still stable [103]. Diamond-based film with sensing function has been widely applied and can also be used in wearable sensors in the future. A cellulose nanofibers (CNF)/nanodiamond (ND)/MXene (CNM) composite film introducing ND via vacuum-assisted self-assembled method was produced [123]. Nacre-like structure and strong hydrogen bonding between MXene and CNF endow satisfactory mechanical properties (89.14 ± 3.61 MPa). It is demonstrated that the central surface temperature of LED/CN10M30 rises to 100.4 °C at 30 s, and the temperature difference is 3.7 times that of bare LEDs. Therefore, the above results demonstrate that the CNM composite films have excellent auxiliary heat dissipation capacity, which can greatly improve reliability and extend its service life. Wang et al. [124] prepared poly-(diallyldimethylammonium chloride)-functionalized nanodiamond (ND@PDDA)/aramid nanofiber (ANF) composite films using a self-assembly strategy. Owing to a strong interfacial interaction arising from electrostatic attraction, ND particles attract strongly along the ANF axis to form ANF/ND “core—sheath” arrangements. Thanks to this structure, the incorporation of ND@PDDA can significantly protect the ANF fibrils and improve the thermal stability of the composite film. The heat-resistance index (THRI) of the 50 wt % ND@PDDA/ANF composite film reached 279.33 °C, which was 31.59 °C higher than that of the pure ANF film (247.74 °C). The improved thermal stability enables the ND@PDDA/ANF composite films to operate normally under high temperature conditions without thermal decomposition. Notably, this nanofiber showed outstanding flame retardancy. Flame retardancy is required for applications in high temperature environments. A pure ANF film and a 50 wt % ND@PDDA/ANF composite film were exposed to a flame in air (Figure 6a,d). The pure ANF film ignited and was completely burned out within 3 s (Figure 6b,c). Figure 6 indicated the 50 wt % ND@PDDA/ANF composite film kept its initial shape and exhibited nonflammable behaviors owing to the protection provided by ND@PDDA.

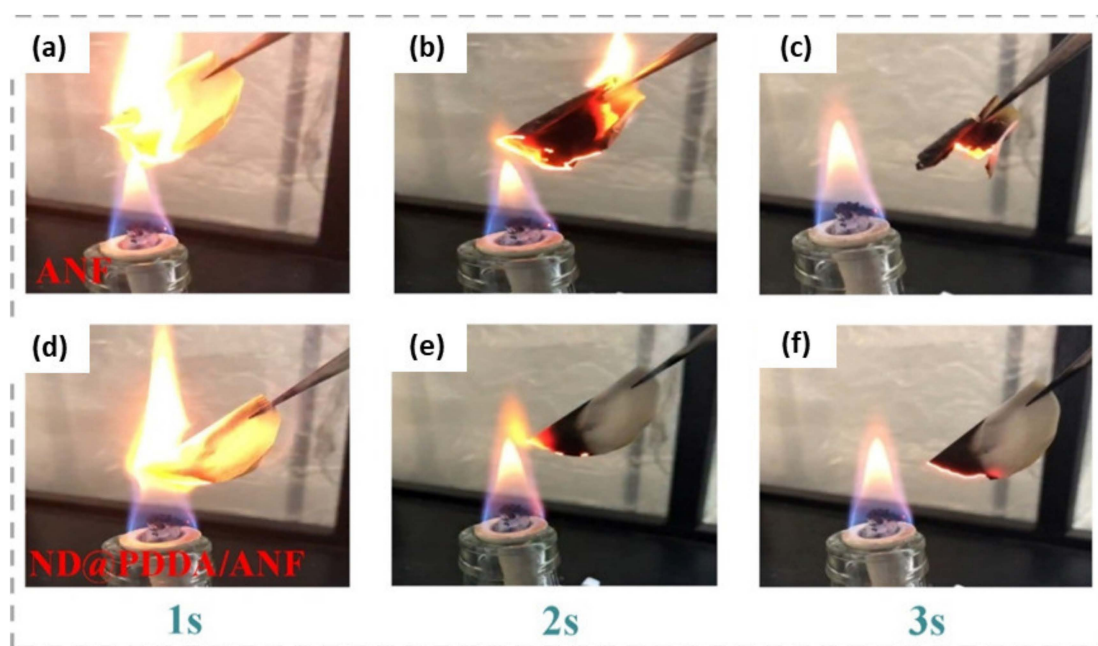


Figure 6. (a–e) Images showing flame test of the pure ANF film. (a–f) Images showing flame test of the 50 wt % ND@PDDA/ANF film [124].

5. Carbon Materials Based Strain Sensors on Extreme Humidity or Other Harsh Condition

Current strain sensors still face challenges such as being prone to failure under humid or cold conditions, lack of washing durability and chemical fragility. Exploration of wearable strain sensors in diverse application scenarios is one global requirement for shaping the future of our intelligent community. Apart from extreme temperatures, most strain sensors suffer from the constraint of operation in dry environments due to susceptibility to chemical corrosion or interference in humid circumstances [125,126]. Recently, the fabrication of strain sensors with higher sensitivity and larger detection areas has received considerable attention [55,85,127], but few studies have focused on wearable sensors under extreme conditions, such as intense UV irradiation, large diurnal temperature differences, or extremely cold weather. The exploration of strain sensors with mechanical and chemical robustness, or with the function of water repellency, enables a sensing coverage with a broader application scenario to revolutionize our future [128,129]. For example, a strain sensor with chemical resistivity can be potentially applied for a human machine interaction system as the operation tool even under harsh conditions. A device with waterproof capability also enables underwater applications by transducing the mechanical behaviors, e.g., anger bending, to electrical signals for communications that are difficult to achieve via sound waves [99].

5.1. CNT-Based Strain Sensor on Extreme Humidity or Other Harsh Condition

A flexible film with a sandwich-like structure consisting of thermoplastic elastomer (TPE), multiwalled carbon nanotubes (MWCNTs), and polydimethylsiloxane (PDMS) showed extreme repellency to water, salt, acid, and alkali solutions [107]. In this study, the film was dipped in these solutions and the conductivity was measured every 5 min for 60 min. Figure 7a shows that the resistance of the film sustained around 4.15–4.20 K Ω without obvious change in water, acid, alkali, and salt solutions. This may be due to the air layer trapped on the surface which can inhibit the attack of acid or alkali. After the film was immersed in water, salt, or acid/alkali solutions for 7 days, and then rinsed with water and dried at 60 °C, the contact angle (CA) of the film still remained above 156° (Figure 7b), indicating excellent durability of super-hydrophobicity to acid, alkali, salt, and water solvents corrosion. Moreover, Gao et al. [98] reported a strain sensor that displayed outstanding long-term stability, because CAs and surface resistance of this kind of sensor varied little when dipping it in water, acidic, and alkaline solutions. It is coated by a CNT/SiO₂ that can be used under moist, acidic, or other harsh conditions without sacrificing its conductivity and super-hydrophobicity, displaying outstanding anti-corrosion properties. A highly stretchable and sensitive strain sensor made of CNT–PDMS nanocomposites showed relative stability in high humidity environments [116]. Another water-resilient strain sensor was developed: an SWCNT was encapsulated in a non-fluorinated superhydrophobic coating, providing water resistance during elastic deformation [93,101]. Notably, the water-repellence was maintained in corrosive environments, such as in acidic, alkaline, or saline aqueous solutions, evidencing its applicability in harsh environments. Moreover, some strain sensors showed humidity-resistance, temperature-resistance, and ethane-resistance at the same time. CNT/CB composites show outdoor usage robustness, including excellent salt-spray resistance, hot-humidity stability, and a wide operation temperature range of –40 to +50 °C [120]. It is seen that the modulus of the samples both maintains the constant at the work temperature range between –40 and +50 °C (Figure 7c). It is noticed that the resistance barely changes for the whole temperature range (Figure 7d). The electrical resistance exhibits only a tiny increase of 0.13% when the composites suffer water vapors at the temperature of 60 °C and at a relative humidity of 75% (Figure 7e). Their liquid resistance was identified by the two liquids of water and ethane, common in our daily lives. After they were completely immersed for one day at room temperature, the resistance variations were only 0.5% and 2.6% for water and ethane (Figure 7f). It

is really important that CNT/CB composites have desirable ambient environmental resistance to serve their sensor applications [130–133].

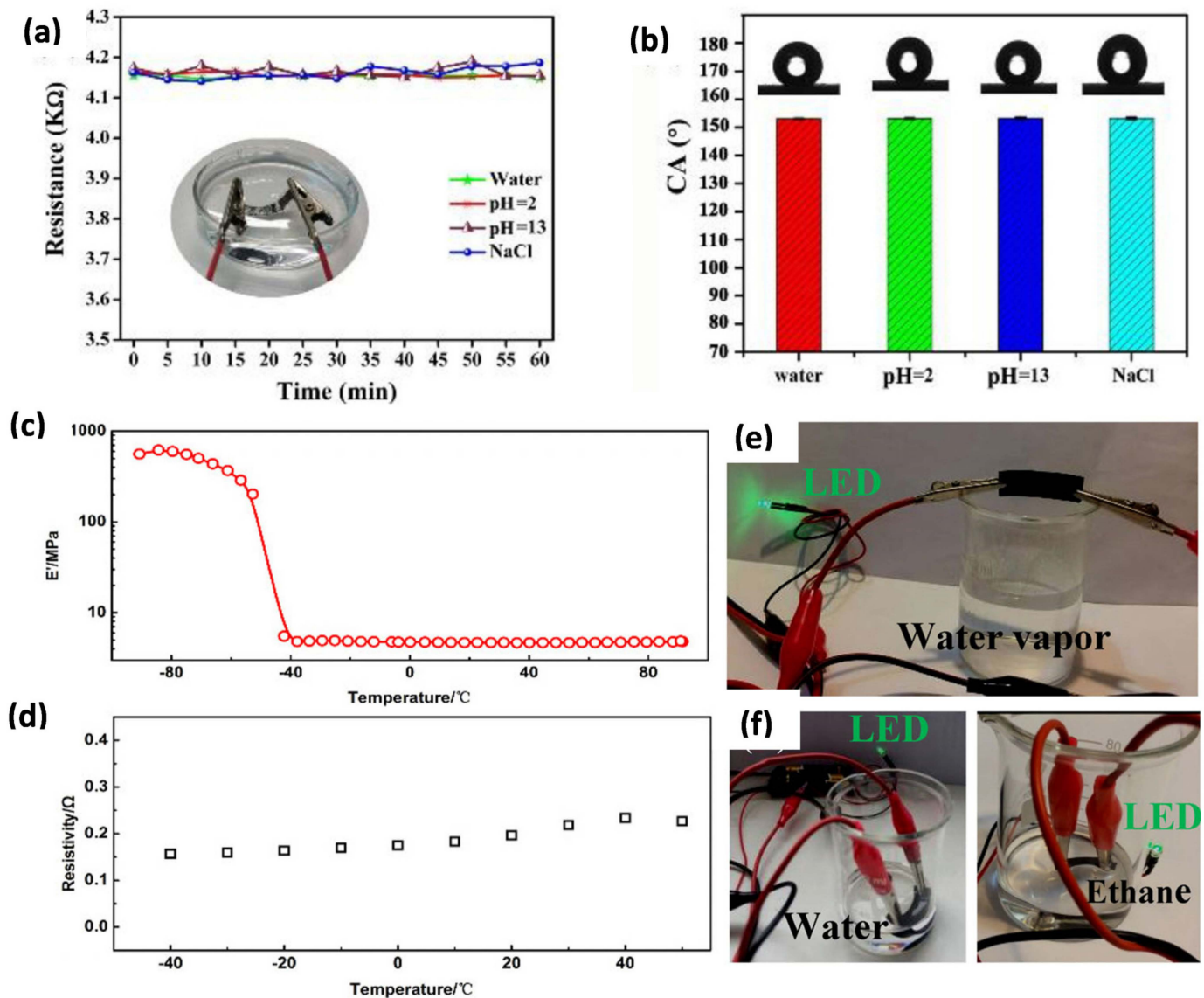


Figure 7. (a) Conductivity stability test of the film in water, acidic (pH = 2), alkaline (pH = 13), and salt solutions. Inset of shows the “silver mirror” phenomenon in water and test status of the film. (b) CA of the functional film after immersion in different solutions for 7 days [107]. (c) The dependence of storage modulus E_0 on the temperatures of -80 to $+80$ °C. (d) Resistivity of the CB/CNT composite in the temperature range of -40 to $+50$ °C. (e,f) A self-made device with the composite sample and LED lights is placed in the water vapor with a temperature of $+60$ °C and a humidity of 75% and is immersed in water and ethane for 1 day. The brightness of the LED light does not change during the two processes [120].

5.2. Graphene Based Strain Sensor on Extreme Humidity or Other Harsh Condition

A reduced graphene oxide (rGO) conductive fabric was first obtained by electrostatic self-assembly of chitosan (CS), as shown in Figure 8 [102]. A polyamide/spandex knitted fabric (PSKF) $@$ rGO/SiO₂-PDMS sensor showed that the sensor exhibited a broad strain range of 0 to 60% and a negative GF up to -2.08 , with excellent cycling stability and durability during 4000 linear strain cycles. Importantly, this sensor was superhydrophobic and resistant to chemical corrosion, enabling its use in high humidity and low temperature environments and hazardous scenarios. When the fabric sensor

was submerged in water, ethanol, toluene, hexane, acetone, hydrochloric acid aqueous solution (pH = 1), and sodium hydroxide aqueous solution (pH = 13) for 24 h, the water contact angles (WCA) of the fabric sensor surface showed only a negligible decrease and remained above 150° , indicating good durability of the fabric sensor against various types of chemical corrosion (Figure 8b). In addition, the laundry endurance of the fabric sensor was further assessed with reference to the national standard (GB/T 12490-2014). Although the WCA of the fabric surface gradually decreased with accumulated washing cycles, the fabric surface still maintained its super-hydrophobicity even after ten washing cycles. Zhu et al. reported an environment-tolerant strain sensor made by incorporating hierarchical cellulose nanocrystal/graphene (MCNC-GN) nanocomplexes into a polydimethylsiloxane (PDMS) matrix [108]. The assembled strain sensor possessed a favorable sensitivity, stretchability, durability, and environment stability. The harsh environment resistance of composite elastomers was evaluated by a series of water resistance and UV irradiation tests. The composite elastomer exhibited a hydrophobicity with a water CA (WCA) of 118° (Figure 8c). Even under more severe conditions, such as dyed acid solution (pH = 1), alkaline solution (pH = 14), and salt solution (pH \approx 6), the sub-spherical droplets could maintain their original shape and stand on the sample surface with an average CA of 117° . This suggested that the composite elastomer possessed a stable hydrophobicity and resistance to corrosion, although the CA value was not higher due to the oxygen groups on the surface of the elastomer composite. After a seven-day artificial sweat treatment, the water droplet on the elastomer surface still formed a regular sub-sphere shape with a WCA of 109° . The electrical conductivity was almost constant with a slight fluctuation (Figure 8d), indicating the stable conductivity and hydrophobicity of the elastomer in the human sweat environment. Besides, the elastomer exhibited a favorable aging resistance property. The WCA and electrical conductivity could almost keep a constant value after 5 h UV irradiation (Figure 8e). Zhu et al. [99] developed a direct ink writing (DIW) assembly approach for fabricating fiber-shaped strain sensors by incorporating graphene/CNT hybrid fillers into the silicone elastomer. The proposed fiber-shaped GCE strain sensors exhibit a tolerable strain over 300%, high sensitivity (100% strain, GF = 14,550.2), and high durability (10,000 loops), and can maintain excellent electromechanical stability to environmental temperature change (reaching at 60°C) and show good long-term (30 days) environmental stability and waterproof characteristics. Apart from the temperature-resistance ability, a GMF sensor remains stable at a relative humidity of \approx 39% and fluctuates moderately with increasing relative humidity up to \approx 71%, which shows that the GMF sensor is insensitive to humidity changes, owing to the reduction in functional groups [122].

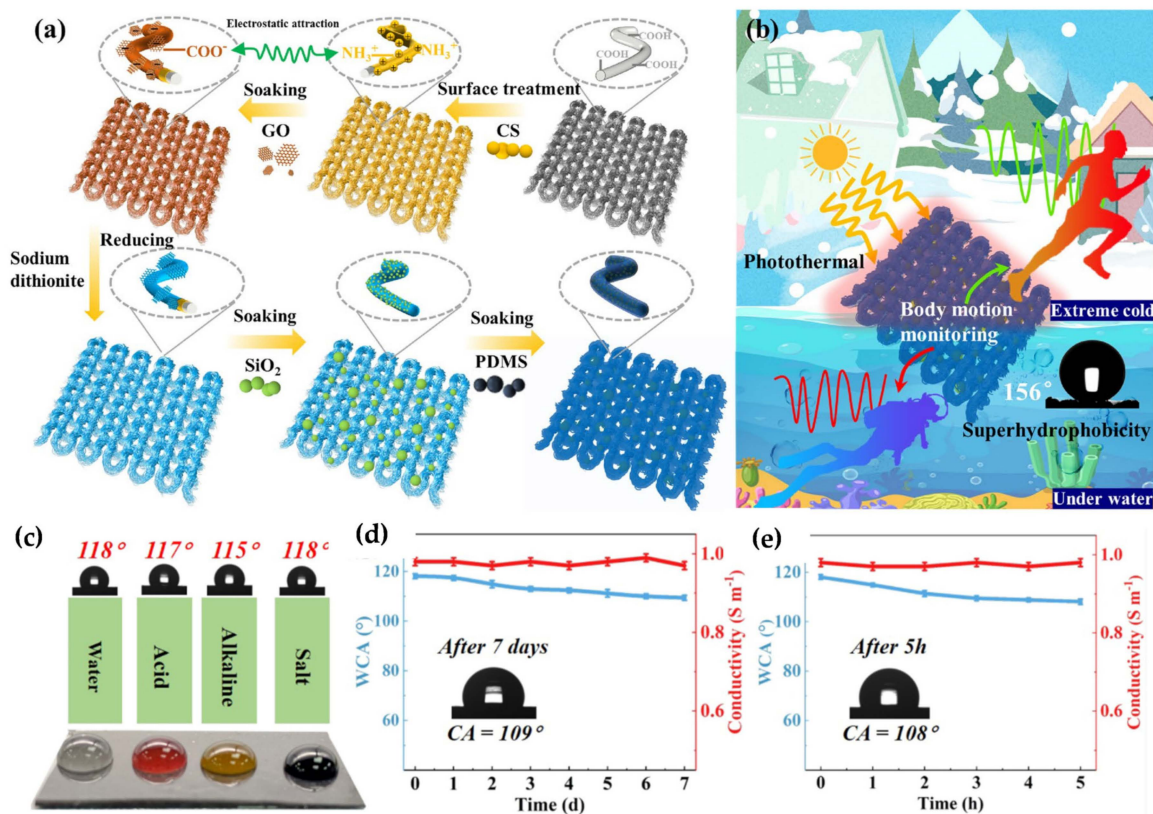


Figure 8. (a) A Schematic illustration of the preparation process of the PSKF@rGO/SiO₂-PDMS sensor. (b) Schematic diagram of the application scenarios and functions of the PSKF@rGO/SiO₂-PDMS sensor [102]. (c) CAs and photographs of various aqueous droplets on the surface of MCNC-GN/PDMS-2. (d) WCA and conductivity variations of the MCNC-GN/PDMS-2 as a function of the immersion time in artificial sweat. Inset: WCA image after a 7-day immersion. (e) WCA changes of MCNC-GN/PDMS-2 with different light irradiation time. Inset: WCA image after a 5 h UV irradiation.

5.3. Nanodiamonds Based Strain Sensor on Extreme Humidity or Other Harsh Condition

A flower-like molybdenum disulfide (MoS₂)/nanodiamond (ND) nanocomposite was successfully prepared via an easy hydrothermal synthesis method and fabricated into humidity sensors to investigate its humidity sensing characteristics, and it could be seen that it was stable at a humidity from 11% RH to 97% RH [106]. A smart multifunctional fabric was produced from the combination of ND with polyaniline (PAIN) with improved mechanical and comfort properties [104]. The nanocomposites based on ND and PAIN are still present on the surface of the fabric even after five commercial washing cycles, which could be due to the bond formation between the nanocomposites and the fabric. The fabrics were washed according to the ISO 105-C08 method. Briefly, the fabrics were washed five times using 20 mL/g liquor-to-fabric ratio at 40 °C for 30 min along with 25 steel balls. ND-PANI showed significant enhancement in abrasion resistance as ND has high abrasion resistance and can increase the abrasion resistance and strengthen the mechanical properties, absorbing the applied energy during abrasion [134,135]. Recently, a pressure sensor device was made of a locally synthesized diamond layer [105]. The rear side of a pressure sensor diaphragm was prepared with an additional diamond layer as protective coating against harsh media, because of the diamond's chemical inertness and resistance.

6. Applications

Carbon material (carbon nanotubes, graphene, and nanodiamond) strain sensors exhibit unique properties and resilience, making them highly versatile in harsh environments. These sensors find diverse applications in healthcare, including human motion

sensing, health monitoring, electronic skins (E-skin), and special applications. Integrated into wearable devices, they enable continuous monitoring of vital signs, body movements, and muscle activity, even during rigorous physical activities, thanks to their flexibility and ability to withstand mechanical stresses. In healthcare settings, particularly in monitoring and diagnostics, carbon-based strain sensors, such as those using carbon nanotubes, graphene, and nanodiamond, prove to be well-suited due to their sensitivity, flexibility, and durability. Their integration into various healthcare applications, such as wearable health monitoring devices, orthopedic monitoring, pressure ulcer prevention, smart implants, rehabilitation, cardiac monitoring, prosthetics, and surgical robotics, enables real-time monitoring, precise diagnostics, and customized treatment plans, ultimately enhancing patient care and healthcare outcomes. As research and technology progress, carbon material strain sensors are expected to play an increasingly vital role in healthcare applications, further revolutionizing patient care and healthcare practices.

6.1. Motion Sensing

The wearable sensor serves as a crucial component determining the functionality of current smart devices. However, existing monitoring equipment based on physical indicators like explosive force, respiration, heart rate, blood oxygen saturation, and electromyography lacks wear comfort and sensitivity. Consequently, real-time monitoring of athletes' physical information during free movement is hindered, affecting accurate motion parameter data and ultimately impacting training effectiveness. Thus, there is an urgent demand for the development of flexible wearable strain sensors that offer comfort and high sensitivity, enabling real-time monitoring of athletes' status. To achieve real-time health data during exercise, wearable sensors are strategically placed on various body parts, such as elbows, wrists, fingers, pulses, and knees, facilitating continuous and precise monitoring.

Especially for some outdoor activities, activities take place in an extreme situation, such as at low temperatures or in high humidity. Ma et al. [45] reported that a CNT-based strain sensor exhibits excellent temperature tolerance ($-40\text{ }^{\circ}\text{C}$) and long-lasting moisture (20 days). After being stored at $-40\text{ }^{\circ}\text{C}$ for 24 h, the anti-freezing organohydrogel maintained sensitivity and could be assembled as a wearable device to monitor human biologic activities at low temperatures. In addition, Lu et al. [102] report that a PSKF@rGO/SiO₂-PDMS sensor expands the working range. For instance, athletes can use this PSKF@rGO/SiO₂-PDMS sensor to detect their finger, wrist, elbow, knee, and ankle movements and different movements (walking and running) of the same joint were also detected (Figure 9a–g). A resistance curve with high repeatability was still observed even when the fabric sensor was submerged in water or placed in a severely cold environment, indicating that the fabric sensor could still maintain good mechanical and electrical properties, as shown in Figure 9h,i. Furthermore, due to its super-hydrophobicity, the fabric sensor maintained normal operation even after water was poured on it and when activity was monitored in sweaty conditions. Based on its multiple superior properties, this sensor could be used as winter sportswear for athletes to track their actions without being impacted by water and as a warmer to ensure the wearer's comfort.

A kind of sensor could detect minor motion. The polypyrrole (PPy)/single-walled carbon nanotube (SWCNT)/polydopamine(PDA)/cotton composite was employed to capture subtle motions originating from the vocal cords during drinking, as depicted in Figure 9 [121]. Remarkably, a unique and repetitive $\Delta R/R_0$ response profile was observed when the volunteer drank 100 mL of orange juice in four sips, highlighting the composite's potential to sense complex and delicate motions of the vocal muscles (Figure 9j). To monitor tiny motions arising from wrist movement during writing, the same composite was applied to the wrist region of the right hand. The sensor's response was examined while writing four different words, "CTN", "PDA", "CNT", and "PPy", with each word showing a distinctive, repetitive, and reproducible $\Delta R/R_0$ response (Figure 9k).

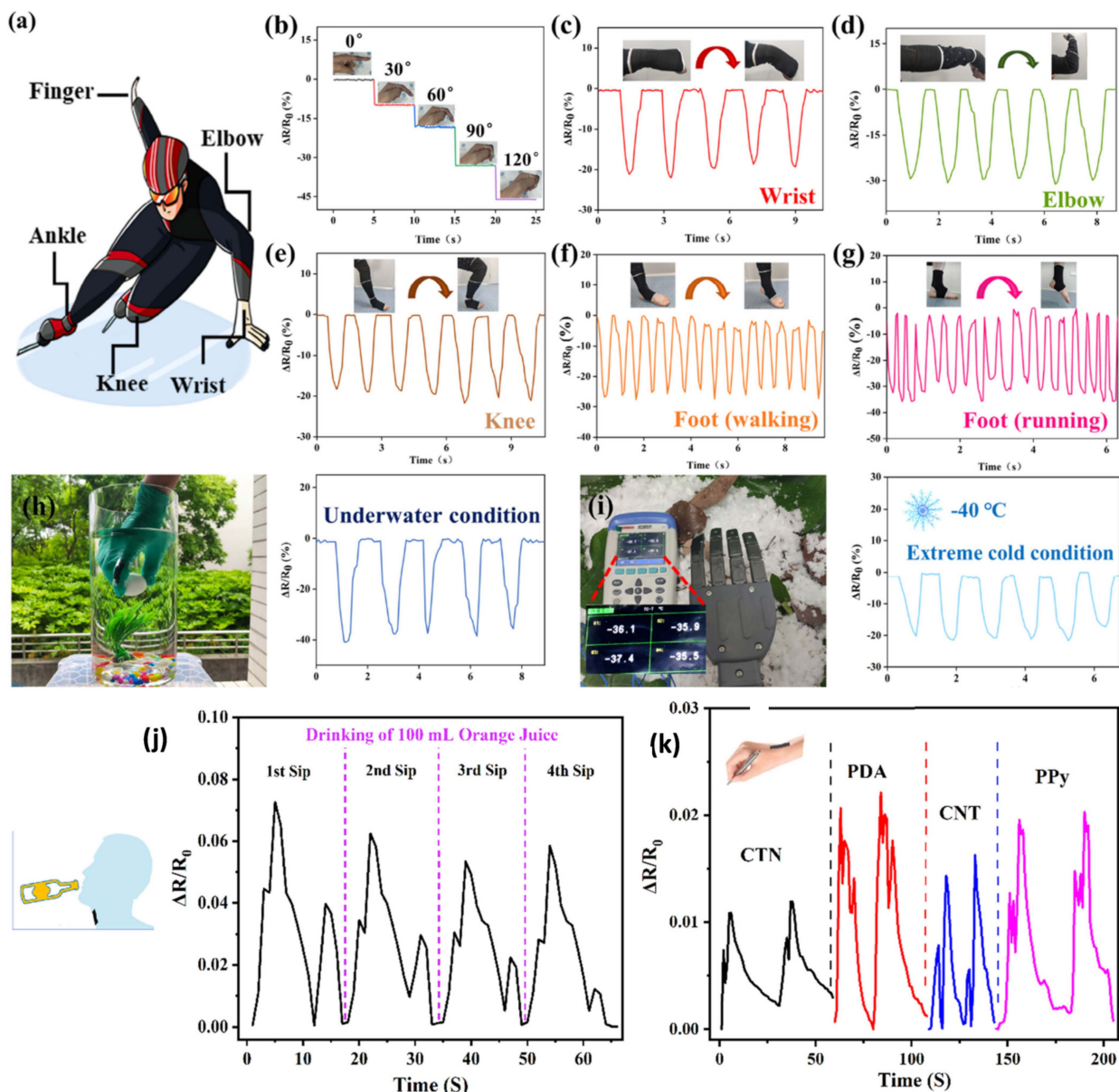


Figure 9. (a) Schematic illustration of the PSKF@rGO/SiO₂-PDMS sensor mounted on human joints for exercise monitoring and management. (b) Relative resistance variation of the PSKF@rGO/SiO₂-PDMS sensor based on finger bending at a certain angle. Insets: photos of an index finger at angles of 0°, 30°, 60°, 90°, and 120°. (c–g) Real-time relative resistance variation of the PSKF@rGO/SiO₂-PDMS sensor when monitoring continuous motions of the wrist, elbow, knee, and foot while walking and running. (h,i) Real-time relative resistance variation of the PSKF@rGO/SiO₂-PDMS sensor under extreme conditions (underwater or extremely low temperature (−40 °C)) [102]. (j) The strain sensing performance of the PPy/SWCNT/PDA/cotton composite on the index finger; changes of $\Delta R/R_0$ while drinking; (k) the sensor attached on the wrist; $\Delta R/R_0$ change profile during writing [121].

6.2. Health Monitor

In the fields of epidemiology and disease control, the use of carbon materials-based flexible strain sensors is vital and essential. In athletic training, real-time recording and analysis of bio-signal signals, including respiration, heart rate, and electromyography, are vital. As a result, they serve as ideal health indicators, playing a crucial role in monitoring public and personal health with precision.

An example of sensor designs for detecting the pulses of the wrist is based on MWCNT [107]. The superhydrophobic sensors were applied to various positions on individuals' skin to facilitate real-time detection. As depicted in Figure 10a, the sensor adhered firmly to the wrist surface, enabling the detection of tiny deformations caused by pulse vibrations and producing a sensitive and stable wrist pulse signal. The amplified image displayed in Figure 10a showcases a typical radial artery pulse waveform with three distinct peaks, affirming the sensor's suitability for human health testing. Moreover, in addition to its capability for precise individual detection, the sensor exhibits high sensitivity in recognizing human joint movements. A flexible and multifunctional temperature/pressure/loading composite foam sensor was developed [97]. Figure 10b,c demonstrate that the PDA-CNT/PDMS sensor exhibits continuous and stable signal peaks with higher intensity compared to the CNT/PDMS sensor when detecting pulse waves, including those from the left superficial temporal artery and the left carotid artery. This strain sensors can also be assembled on a face mask to measure human breathing. To showcase the potential application of the PDA-CNT/PDMS composite sensor, Figure 10d illustrates a flexible composite microarray sewn inside a medical mask to create a smart mask. When an adult breathes with this mask, the inhaled hot air comes into contact with the microarray, leading to a decrease in sensor resistance (Figure 10d). Consequently, the sensor can monitor the human body's breathing rate in relation to exercise and health. Figure 10d displays distinct signals representing normal breathing and shortness of breath, empowering the PDA-CNT/PDMS composite sensor with the capability to predict early diseases in the human body. Moreover, a breath sensor based on rGO-CGY and elastic yarns can monitor speaking, coughing, and breathing [122]. The electrical pattern obtained during gum chewing, as shown in Figure 11a, exhibits reproducibility, revealing its promising application prospects in oral locomotion and training. We affixed the sensor to the throat to discern coughing and speaking states. Figure 11b depicts the resistance change of the sensor during coughing, showing an upward and downward resistance change signal linked to the exertion and release of cough, respectively, consistent with corresponding epidermal vibrations. Furthermore, the electrical response remains highly repeatable with minimal deviations, indicating precise tracking of motion with a reproducible signaling pattern. In Figure 11c, the sensor effectively captures resistance signals generated during speech, exhibiting distinguishable and reproducible patterns when speaking different words ("I love you", "strain sensor", and "wearable"). Additionally, signals of normal human breathing and breathing during running are presented in Figure 11d, showcasing discernible respiratory rates and depths under the two diverse conditions.

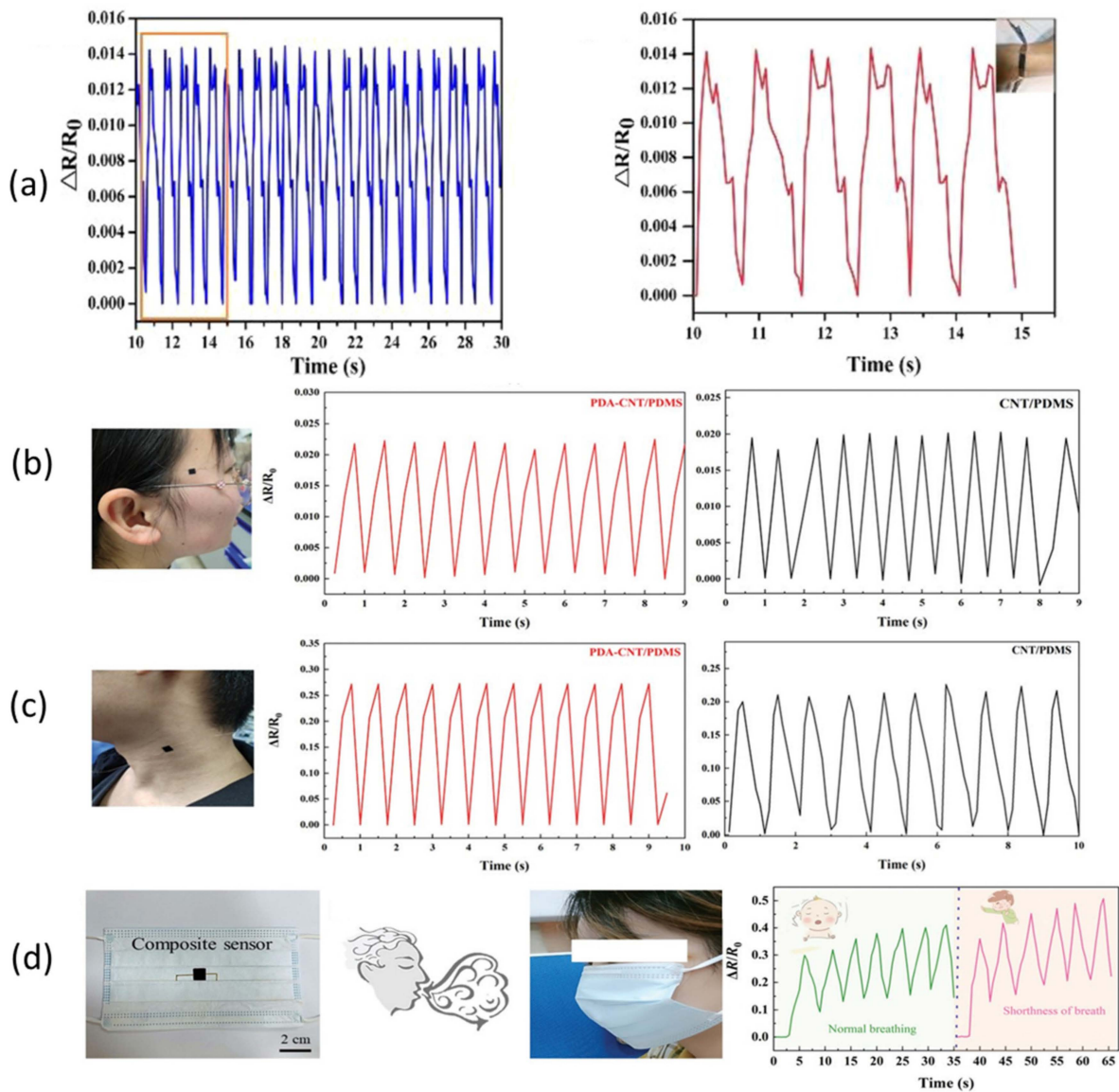


Figure 10. (a) Real-time detection of the wrist pulse when the film self-adhered to the wrist surface and the enlarged image of the pulse detection [107]. (b,c) Comparison of the signals from the CNT/PDMS and PDA-CNT/PDMS composite sensors for recording the left superficial temporal artery and left carotid artery. (d) Photograph of a medical mask with a flexible composite microarray inside. Cartoon diagram of breathing. Photograph of breathing with a medical mask embedded with a flexible composite microarray. Comparison of the signals from the medical sensory mask under normal breathing and shortness of breath of the human body [97].

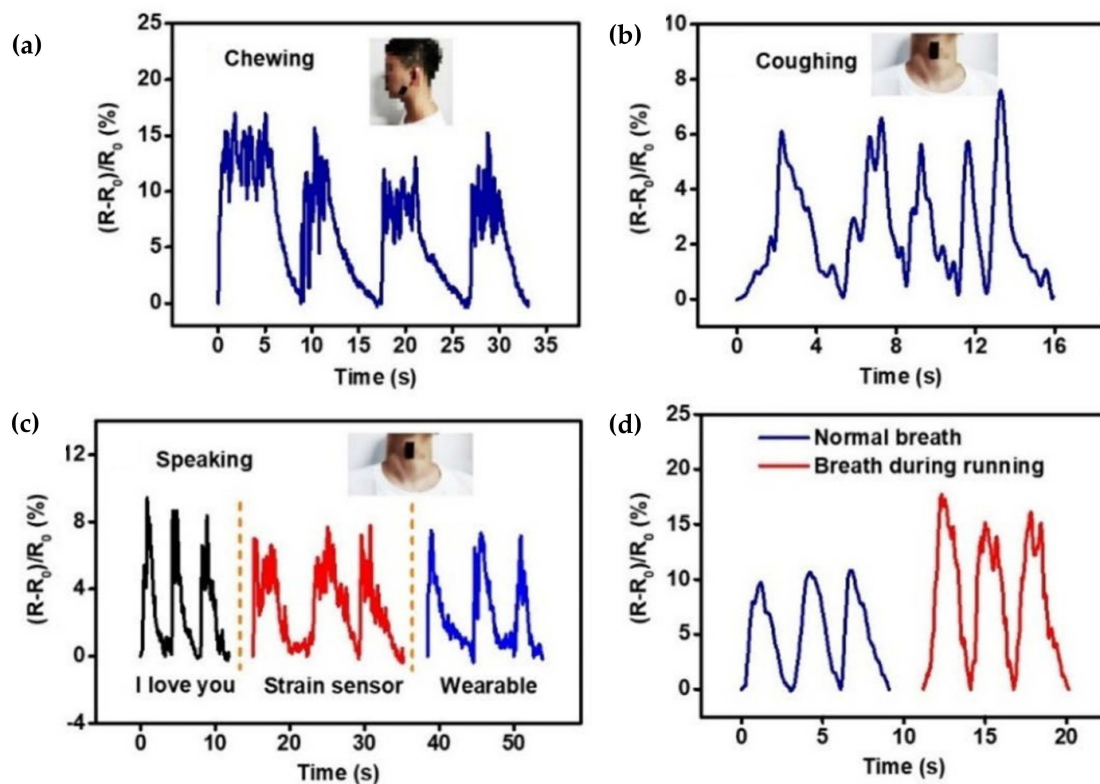


Figure 11. Application demonstration of the GMF sensor. (a) Corresponding signals of chewing gum. (b) Relative electrical resistance changes of throat vibration during coughing. (c) Signals of the throat epidermis vibration while speaking different words. (d) Relative electrical resistance changes during normal breathing and breathing during running [122].

6.3. E-Skin

As a tissue directly in contact with the external environment, the skin can perceive various external stimuli simultaneously. Extensive research has been conducted on its intriguing properties, including self-healing capabilities. In the context of artificial intelligent skin, carbon nanotube-, graphene-, and nanodiamond-based flexible strain sensors emerge as excellent candidates, benefiting from the unique strengths of stretchability and conductivity. These sensors are poised to fully replicate the functions of human skin, and several designs with multi-sensing abilities, such as strain and pressure, temperature and strain, have been developed to achieve this goal.

A polyimide (PI)/carbon nanotubes (CNT) composite aerogel was developed as E-skin [113]. Wearable pressure sensors are widely integrated into smart E-skin systems to detect pressure distribution and the location of mechanical stimuli. Figure 12A,B showcase the schematic illustration and top view of the E-skin, consisting of 5×5 pixels. As illustrated in Figure 12C, the E-skin accurately recognizes the compressed points by recording resistance variation in a two-dimensional (2D) map based on different applied pressures at various locations (with darker colors representing larger resistance variations) when a finger presses the E-skin affixed to the back of the hand. Moreover, a three-dimensional (3D) pressure distribution mapping is obtained through nonlinear surface fitting (Figure 12F), clearly highlighting significant pressure differences at different points. Specifically, the resistance variation in the pressure center amounts to about 34.2%, equivalent to a pressure of approximately 50 kPa. In addition, when the E-skin is gripped with a stone ball in the hand (Figure 12D,E), it also provides a substantial sensing response, with a 3D pressure distribution mapping shown in Figure 12G,H. Overall, these findings demonstrate the promising capabilities of the E-skin for accurately mapping pressure distribution and location. Moreover, Sun et al. [92] assembled a 4×4 electronic fabric using the superhydrophobic conductive RB (based on carbon

nanotubes(CNTs)/reduced graphene oxide (rGO) dual conductive layer) to explore its application in the tactile sensing field (Figure 13a). By pressing the fabric with a figure (Figure 13b) or placing a doll (Figure 13c) on it, the deformation of the conductive RB resulted in resistance changes at different cross points, revealing the corresponding spatial pressure distribution. This was effectively captured through a 3D resistance variation mapping (Figure 13e,f), showcasing the immense potential of our superhydrophobic conductive RB for advanced electronic skin applications.

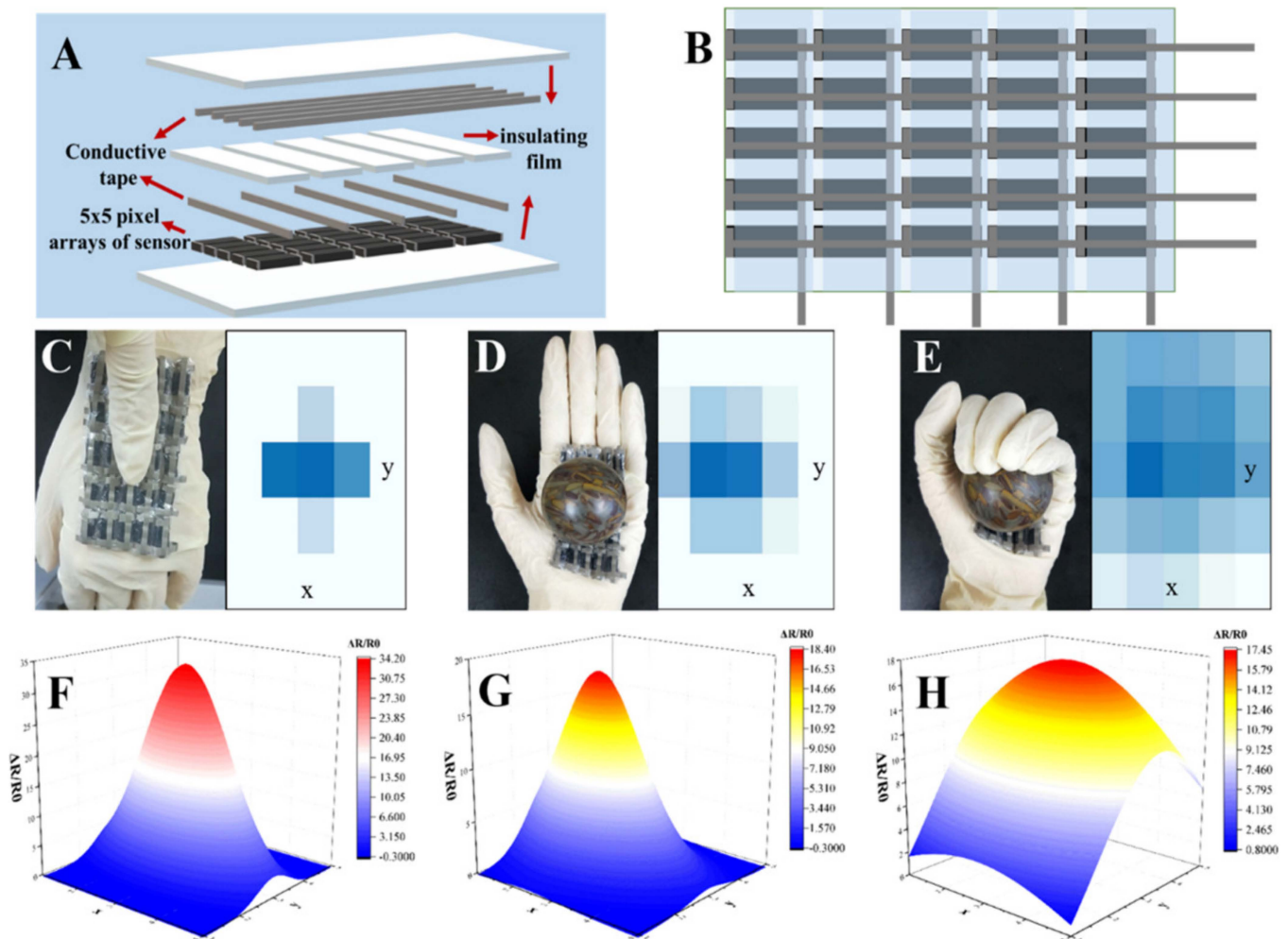


Figure 12. (A) Schematic illustration and (B) top view of the E-skin assembled from the PI/CNT composite aerogel with a size of 5×5 pixels. (C) Photograph of a finger pressing the E-skin attached to the back of the hand and the corresponding resistance variation in a 2D map. Photographs of a stone ball (D) in the hand and (E) being gripped, and their corresponding resistance variation in a 2D map. (F–H) Corresponding pressure distribution mappings over a 3D area of (C–E) based on the change in resistance, respectively [113].

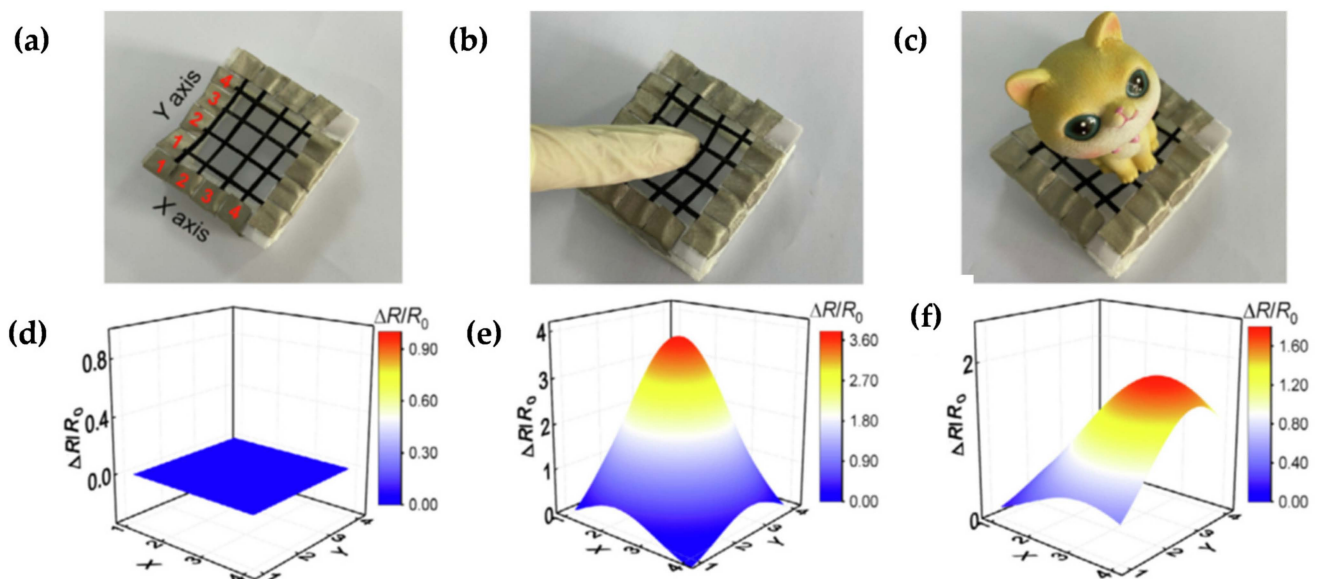


Figure 13. Digital photographs and the corresponding pressure distribution based on the resistance change of (a,d) electronic fabric assembled from the superhydrophobic conductive RB with 4×4 pixels, and (b,e) a finger and (c,f) a doll on the electronic fabric.

6.4. Other Application

6.4.1. Intelligent Logistics, Disaster Rescue, and Space Applications

Beside the above-mentioned applications, there are some special applications for strain sensors in harsh environments. For nuclear or space applications, radiation resistance is imperative, allowing sensors to endure without degradation. Ma et al. [109] reported that a MWCNT/polyimide aerogel exhibited desirable EMI SE values (from 99.4 dB to 46.9 dB when CPIA-4 was compressed from 10 mm to 5 mm) with stable electrical responsiveness across a wide temperature range (from 25 to 316 °C). These materials, therefore, showcase great promise as smart high-temperature EMI shielding materials for radar equipment, satellites, or aerobot landing protection equipment. Moreover, the strain/pressure sensing and EMI shielding performance of the hybrid CNT-coated carbonized melamine foams (CNT/CMFs) were systematically investigated, showing an exceptional EMI shielding effectiveness and a high specific shielding effectiveness of 6147.3 dB cm²/g with an absorption-dominant shielding mechanism due to the highly porous structure [119].

In Shak Sadi's study, to verify the potentiality of the PPy/SWCNT/PDA/Cotton composite as a component of a wearable heating device, the sample was attached to the index finger position of a hand glove while both ends of the composite were connected to an external DC voltage source (2 V) (Figure 14a) [121]. Within 30 s of heating, there was a very uniformly distributed profile of the surface. A component of wearable heating devices is to control the region-specific temperature of the human body as desired by the wearer. Robots with sensors are expected to play a crucial role in extreme environment tasks in the future, such as intelligent logistics, disaster rescue, and aerospace applications [53,54]. The fabric sensor-equipped mechanical arm was carefully maneuvered to approach both a hazardous chemical bottle and a toy doll [102]. The sensor demonstrated its responsiveness, detecting the grasping action regardless of the materials' hardness or softness (see Figure 14b). When the robot successfully grabbed an object, the fabric sensor experienced compression and pressure, leading to a sudden drop in resistance, which promptly activated the signal lamp. Upon releasing the object, the lamp returned to its original state. These results affirm the suitability and reliability of the PSKF@rGO/SiO₂-PDMS fabric sensor even in challenging and demanding application conditions [102].



Figure 14. (a) Demonstration of the wearable heating system, attachment of the composite with a hand glove as a wearable heater; temperature response of the heater on the index finger under 2 V [121]. (b) PSKF@rGO/SiO₂-PDMS sensor mounted on a robot hand for executing dangerous tasks and intelligent logistics [102]. The background of Figure 14b is the university name for the author in reference [111].

6.4.2. Non-Contact Smart Control

A flower-like nanocomposite of molybdenum disulfide (MoS₂) and nanodiamond (ND) was utilized to create humidity sensors [106]. This innovative non-contact sensing control method allows for adjusting the brightness of LED lights by monitoring water evaporation from the skin, presenting a potential and advantageous approach for controlling the brightness of display screens in phones and computers. Leveraging its impressive sensitivity and rapid response, the sensor was applied to monitor water evaporation from the skin. In Figure 15a, the measurement diagram of the sensor during finger water evaporation is displayed, with a micrometer actuator used to control the humidity sensor's distance from the finger. As the distance between the sensor and the finger gradually decreased, the sensor detected the humidity evaporated from sweat glands, leading to an increase in the sensor's response, as depicted in Figure 15a. The humidity values can be determined, as shown in the figure. Additionally, real-time detection of water evaporation occurred when the finger was rapidly brought close to and lifted from the sensor, as demonstrated in Figure 15a. The sensor could clearly and swiftly detect the subtle changes in relative humidity (RH) released from the skin. On the other hand, when uniformly sliding our finger near the top of the sensor, the sensor showed a slow response, indicating a slow adsorption process of RH on the sensor surface. These experimental results underscore the sensor's excellent response sensitivity in monitoring water evaporation from the skin. Furthermore, a non-contact smart sensing control system was constructed by monitoring water evaporation from the skin, as illustrated in Figure 15b. The system primarily consists of an operational amplifier (IC1) and an inverting operational amplifier (IC2). As depicted

in Figure 15b, the LED light's brightness exhibited different degrees of variation with decreasing distance between the finger and the sensor. In comparison to other control methods, this non-contact smart control system offers the added advantage of reducing the risk of bacterial transmission.

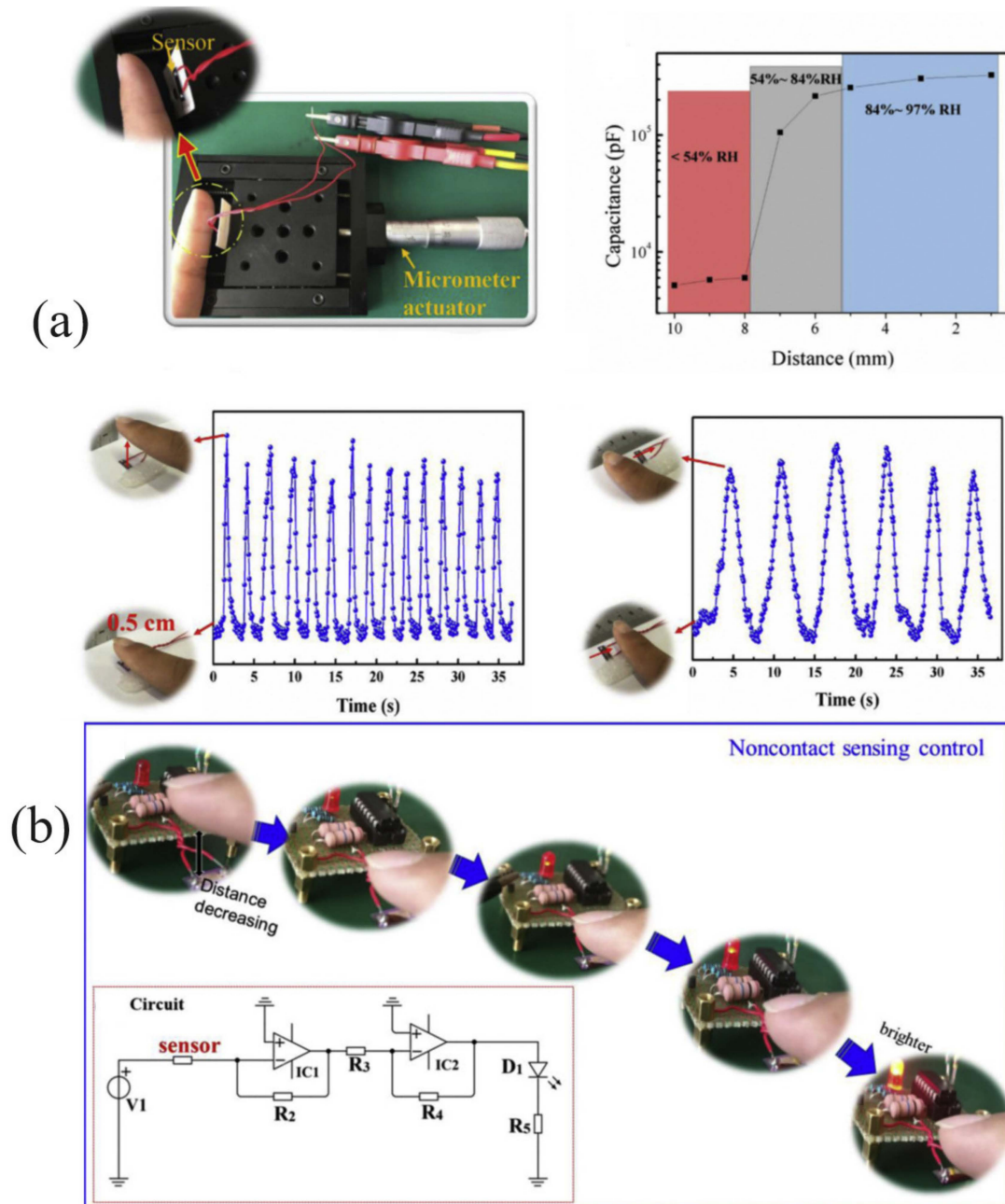


Figure 15. (a) The measurement diagram of the sensor on finger water evaporation. The response to a bare finger with different distances. Real-time detection of water evaporation from a finger, moving up and down, uniform sliding. (b) Noncontact sensing control. The schematic circuit diagram of noncontact sensing system. The photograph of a finger noncontact humidity control system, displaying the different degrees of brightness of a LED light with the decreasing of distances between the finger and sensor [106].

7. Conclusions and Challenges

A comprehensive evaluation of the carbon-based flexible strain sensor was reviewed and discussed. This paper summarizes the recent breakthroughs in the reasonable fab-

rication, performance, and application varieties of CNTs, graphene, nanodiamond, and related materials toward wearable electronics with high-performance flexibility. Because of their extraordinary properties (e.g., ultra-translucency, good electrical conductivity, thermal stability, chemical stability, superior mechanical flexibility, installation to be designed into different pliable macroscopic morphologies, and easily functionalized), these carbon material (CNTs, graphene, and nanodiamond), and related materials such as MWCNT, SWCNT, GO, rGO, and ultrananocrystalline diamond, enable a wide range of applications for high-sensitivity strain sensors, which are promising for motion sensing, health indicators, E-skin, and intelligent logistics, disaster rescue, and space applications.

Compared to CNTs and graphene, nanodiamond has a much shorter history. Nanodiamond (ND) is a novel nanocarbon material with favorable mechanical properties, remarkable chemical inertness, low dielectric constant, outstanding thermal stability, and biocompatibility. Owing to these desirable characteristics, it has been applied in the environmental, energy, biological, and drug delivery fields. With the development of nanodiamond in biological and biomedical areas in recent years, a natural question that has come up is that of which one is better for making strain sensors. As popular carbon nanomaterials, CNTs, graphene, and nanodiamond share some properties, including excellent mechanic, electronic, and thermal properties. Nanodiamonds have high hardness and wear resistance, but they are not as mechanically flexible as CNTs or graphene. It is obvious that CNTs and graphene have been widely used as strain sensors in harsh environments, while there is not a lot of research about nanodiamond-based strain sensors and most reported research focused on pressure sensors. Despite the progress in CNTs, graphene, and nanodiamond-based strain sensors for extreme conditions, challenges remain in terms of sensitivity, stability, and calibration. Researchers continue to explore new carbon materials, sensor designs, and encapsulation methods to enhance their performance and reliability. Future advancements hold the promise of more extensive applications in harsh environments and can revolutionize safety and efficiency in critical industries. Firstly, maintaining high sensitivity and accuracy of carbon material strain sensors in harsh conditions can be challenging. Extreme temperatures, mechanical stresses, and exposure to corrosive substances might affect the sensor's performance, leading to inaccurate readings. Secondly, harsh environments can alter the properties of carbon materials, affecting their calibration and stability over time. Regular calibration is essential to ensure accurate strain measurements, but this process can be complicated and time-consuming in challenging conditions. Thirdly, prolonged exposure to harsh environments, such as extreme temperatures or corrosive substances, can degrade the carbon material's properties. This degradation may lead to reduced sensor lifespan and performance. Fourthly, integrating carbon material strain sensors into existing structures or systems in harsh environments might be difficult due to size constraints, wiring complexities, and compatibility issues. Harsh environments can introduce various sources of signal interference, such as electromagnetic noise, which can impact the sensor's ability to transmit data accurately. Finally, carbon material strain sensors, particularly those designed to withstand extreme conditions, may be more expensive compared to conventional strain sensors, posing a challenge for their widespread adoption.

Strain sensors are used to measure the deformation of an object under stress. They are widely used in various fields such as aerospace, civil engineering, and medical engineering. The prospects of strain sensors in harsh environments are promising. In recent years, there has been a growing demand for sensors that can withstand harsh environments such as high temperatures, high radiation, high shock, and chemically corrosive environments. TE Connectivity has developed a range of industrial sensors that can withstand harsh environments. These sensors are designed to operate in demanding conditions and provide accurate and reliable data. The latest sensor developments are being influenced by IoT trends including miniaturization, digitization, sensor fusion, lower power, and the integration of wireless communication technologies. The commercialization of strain sensors for harsh environments is already underway. However, the requirements for sensors are becoming more demanding as factories are becoming more autonomous and IoT (Internet of

Things) ready. The development of sensors and actuators to operate in harsh environmental conditions has been gaining momentum in recent years.

Overall, the future prospects of carbon nanotubes, graphene, and nanodiamond as strain sensors in harsh environments are exciting and dynamic. Ongoing research and development efforts are expected to lead to significant advancements in materials, fabrication techniques, and sensor design, making these carbon-based sensors increasingly reliable, versatile, and applicable in a wide range of extreme conditions, including aerospace, automotive, oil and gas, structural monitoring, and healthcare applications. As research continues to push the boundaries of materials science and sensor technology, carbon-based strain sensors are expected to play an increasingly vital role in shaping the future of wearable and flexible electronics, leading to improved healthcare monitoring, industrial applications, and the realization of a smarter, interconnected community.

Author Contributions: All authors contributed equally to this work. All authors have read and agreed to the published version of the manuscript.

Funding: This research was funded by the Jiangsu Science and Technology Programme–Young Scholar (BK20200251) and the XJTLU AI University Research Centre, Jiangsu Province Engineering Research Centre of Data Science and Cognitive Computation at XJTLU and SIP AI innovation platform (YZCXPT2022103).

Data Availability Statement: Data are contained within the article.

Acknowledgments: The authors also acknowledge the support from the State Key Laboratory for Manufacturing Systems Engineering (Xi'an Jiaotong University).

Conflicts of Interest: The authors declare no conflict of interest.

References

- Gao, S.; Zhao, X.; Fu, Q.; Zhang, T.; Zhu, J.; Hou, F.; Ni, J.; Zhu, C.; Li, T.; Wang, Y. Highly transmitted silver nanowires-SWCNTs conductive flexible film by nested density structure and aluminum-doped zinc oxide capping layer for flexible amorphous silicon solar cells. *J. Mater. Sci. Technol.* **2022**, *126*, 152–160. [[CrossRef](#)]
- Li, G.; Wang, L.; Lei, X.; Peng, Z.; Wan, T.; Maganti, S.; Huang, M.; Murugadoss, V.; Seok, I.; Jiang, Q. Flexible, yet robust polyaniline coated foamed polylactic acid composite electrodes for high-performance supercapacitors. *Adv. Compos. Hybrid Mater.* **2022**, *5*, 853–863. [[CrossRef](#)]
- Wang, Y.; Yang, D.; Hessien, M.M.; Du, K.; Ibrahim, M.M.; Su, Y.; Mersal, G.A.; Ma, R.; El-Bahy, S.M.; Huang, M. Flexible barium titanate@ polydopamine/polyvinylidene fluoride/polymethyl methacrylate nanocomposite films with high performance energy storage. *Adv. Compos. Hybrid Mater.* **2022**, *5*, 2106–2115. [[CrossRef](#)]
- Das, H.S.; Roymahapatra, G.; Kumar, P.; Das, R. Study the effect of ZnO/Cu/ZnO multilayer structure by RF magnetron sputtering for flexible display applications. *ES Energy Environ.* **2021**, *13*, 50–56. [[CrossRef](#)]
- Lai, C.; Wang, Y.; Fu, L.; Song, H.; Liu, B.; Pan, D.; Guo, Z.; Seok, I.; Li, K.; Zhang, H. Aqueous flexible all-solid-state NiCo-Zn batteries with high capacity based on advanced ion-buffering reservoirs of NiCo₂O₄. *Adv. Compos. Hybrid Mater.* **2022**, *5*, 536–546. [[CrossRef](#)]
- Wang, R.; Sun, L.; Zhu, X.; Ge, W.; Li, H.; Li, Z.; Zhang, H.; Huang, Y.; Li, Z.; Zhang, Y.F. Carbon nanotube-based strain sensors: Structures, fabrication, and applications. *Adv. Mater. Technol.* **2023**, *8*, 2200855. [[CrossRef](#)]
- Li, Z.; Li, H.; Zhu, X.; Peng, Z.; Zhang, G.; Yang, J.; Wang, F.; Zhang, Y.F.; Sun, L.; Wang, R. Directly printed embedded metal mesh for flexible transparent electrode via liquid substrate electric-field-driven jet. *Adv. Sci.* **2022**, *9*, 2105331. [[CrossRef](#)]
- Shintake, J.; Piskarev, Y.; Jeong, S.H.; Floreano, D. Ultrastretchable strain sensors using carbon black-filled elastomer composites and comparison of capacitive versus resistive sensors. *Adv. Mater. Technol.* **2018**, *3*, 1700284. [[CrossRef](#)]
- Li, X.; Yang, T.; Yang, Y.; Zhu, J.; Li, L.; Alam, F.E.; Li, X.; Wang, K.; Cheng, H.; Lin, C.T. Large-area ultrathin graphene films by single-step marangoni self-assembly for highly sensitive strain sensing application. *Adv. Funct. Mater.* **2016**, *26*, 1322–1329. [[CrossRef](#)]
- Eom, J.; Jaisutti, R.; Lee, H.; Lee, W.; Heo, J.-S.; Lee, J.-Y.; Park, S.K.; Kim, Y.-H. Highly sensitive textile strain sensors and wireless user-interface devices using all-polymeric conducting fibers. *ACS Appl. Mater. Interfaces* **2017**, *9*, 10190–10197. [[CrossRef](#)]
- Ramalingame, R.; Lakshmanan, A.; Müller, F.; Thomas, U.; Kanoun, O. Highly sensitive capacitive pressure sensors for robotic applications based on carbon nanotubes and PDMS polymer nanocomposite. *J. Sens. Sens. Syst.* **2019**, *8*, 87–94. [[CrossRef](#)]
- You, I.; Kim, B.; Park, J.; Koh, K.; Shin, S.; Jung, S.; Jeong, U. Stretchable E-skin apexcardiogram sensor. *Adv. Mater.* **2016**, *28*, 6359–6364. [[CrossRef](#)] [[PubMed](#)]

13. Gong, S.; Lai, D.T.; Wang, Y.; Yap, L.W.; Si, K.J.; Shi, Q.; Jason, N.N.; Sridhar, T.; Uddin, H.; Cheng, W. Tattolike polyaniline microparticle-doped gold nanowire patches as highly durable wearable sensors. *ACS Appl. Mater. Interfaces* **2015**, *7*, 19700–19708. [[CrossRef](#)]
14. Yu, X.; Xie, Z.; Yu, Y.; Lee, J.; Vazquez-Guardado, A.; Luan, H.; Ruban, J.; Ning, X.; Akhtar, A.; Li, D. Skin-integrated wireless haptic interfaces for virtual and augmented reality. *Nature* **2019**, *575*, 473–479. [[CrossRef](#)] [[PubMed](#)]
15. Zheng, M.; Li, W.; Xu, M.; Xu, N.; Chen, P.; Han, M.; Xie, B. Strain sensors based on chromium nanoparticle arrays. *Nanoscale* **2014**, *6*, 3930–3933. [[CrossRef](#)] [[PubMed](#)]
16. Ho, M.D.; Ling, Y.; Yap, L.W.; Wang, Y.; Dong, D.; Zhao, Y.; Cheng, W. Percolating network of ultrathin gold nanowires and silver nanowires toward “invisible” wearable sensors for detecting emotional expression and apexcardiogram. *Adv. Funct. Mater.* **2017**, *27*, 1700845. [[CrossRef](#)]
17. Duan, S.; Wang, Z.; Zhang, L.; Liu, J.; Li, C. A highly stretchable, sensitive, and transparent strain sensor based on binary hybrid network consisting of hierarchical multiscale metal nanowires. *Adv. Mater. Technol.* **2018**, *3*, 1800020. [[CrossRef](#)]
18. Narongthong, J.; Das, A.; Le, H.H.; Wießner, S.; Sirisinha, C. An efficient highly flexible strain sensor: Enhanced electrical conductivity, piezoresistivity and flexibility of a strongly piezoresistive composite based on conductive carbon black and an ionic liquid. *Compos. Part A Appl. Sci. Manuf.* **2018**, *113*, 330–338. [[CrossRef](#)]
19. Seong, M.; Hwang, I.; Lee, J.; Jeong, H.E. A pressure-insensitive self-attachable flexible strain sensor with bioinspired adhesive and active CNT layers. *Sensors* **2020**, *20*, 6965. [[CrossRef](#)]
20. Chen, S.; Wu, R.; Li, P.; Li, Q.; Gao, Y.; Qian, B.; Xuan, F. Acid-interface engineering of carbon nanotube/elastomers with enhanced sensitivity for stretchable strain sensors. *ACS Appl. Mater. Interfaces* **2018**, *10*, 37760–37766. [[CrossRef](#)]
21. Liu, H.; Gao, H.; Hu, G. Highly sensitive natural rubber/pristine graphene strain sensor prepared by a simple method. *Compos. Part B Eng.* **2019**, *171*, 138–145. [[CrossRef](#)]
22. Yang, Y.-F.; Tao, L.-Q.; Pang, Y.; Tian, H.; Ju, Z.-Y.; Wu, X.-M.; Yang, Y.; Ren, T.-L. An ultrasensitive strain sensor with a wide strain range based on graphene armour scales. *Nanoscale* **2018**, *10*, 11524–11530. [[CrossRef](#)] [[PubMed](#)]
23. Ryciewicz, M.; Ficek, M.; Gajewski, K.; Kunuku, S.; Karczewski, J.; Gotszalk, T.; Wlasny, I.; Wyszomolek, A.; Bogdanowicz, R. Low-strain sensor based on the flexible boron-doped diamond-polymer structures. *Carbon* **2021**, *173*, 832–841. [[CrossRef](#)]
24. Lee, H.; Seong, B.; Moon, H.; Byun, D. Directly printed stretchable strain sensor based on ring and diamond shaped silver nanowire electrodes. *Rsc Adv.* **2015**, *5*, 28379–28384. [[CrossRef](#)]
25. Liu, J.; Zhang, H.; Gong, H.; Zhang, X.; Wang, Y.; Jin, X. Polyethylene/polypropylene bicomponent spunbond air filtration materials containing magnesium stearate for efficient fine particle capture. *ACS Appl. Mater. Interfaces* **2019**, *11*, 40592–40601. [[CrossRef](#)] [[PubMed](#)]
26. Zhang, R.; Ying, C.; Gao, H.; Liu, Q.; Fu, X.; Hu, S. Highly flexible strain sensors based on polydimethylsiloxane/carbon nanotubes (CNTs) prepared by a swelling/permeating method and enhanced sensitivity by CNTs surface modification. *Compos. Sci. Technol.* **2019**, *171*, 218–225. [[CrossRef](#)]
27. Kim, H.-J.; Thukral, A.; Yu, C. Highly sensitive and very stretchable strain sensor based on a rubbery semiconductor. *ACS Appl. Mater. Interfaces* **2018**, *10*, 5000–5006. [[CrossRef](#)]
28. Xu, W.; Hu, S.; Zhao, Y.; Zhai, W.; Chen, Y.; Zheng, G.; Dai, K.; Liu, C.; Shen, C. Nacre-inspired tunable strain sensor with synergistic interfacial interaction for sign language interpretation. *Nano Energy* **2021**, *90*, 106606. [[CrossRef](#)]
29. Wrbanek, J.; Fralick, G.; Gonzalez, J. Developing multilayer thin film strain sensors with high thermal stability. In Proceedings of the 42nd AIAA/ASME/SAE/ASEE Joint Propulsion Conference & Exhibit, Sacramento, CA, USA, 9–12 July 2006; p. 4580.
30. Read, I.; Foote, P. Sea and flight trials of optical fibre Bragg grating strain sensing systems. *Smart Mater. Struct.* **2001**, *10*, 1085. [[CrossRef](#)]
31. Zrelli, A.; Ezzedine, T. Design of optical and wireless sensors for underground mining monitoring system. *Optik* **2018**, *170*, 376–383. [[CrossRef](#)]
32. Mattmann, C.; Clemens, F.; Tröster, G. Sensor for measuring strain in textile. *Sensors* **2008**, *8*, 3719–3732. [[CrossRef](#)] [[PubMed](#)]
33. Wang, M.; Mu, L.; Zhang, H.; Ma, S.; Liang, Y.; Ren, L. Flexible strain sensor with ridge-like microstructures for wearable applications. *Polym. Adv. Technol.* **2022**, *33*, 96–103. [[CrossRef](#)]
34. Liu, X.; Wei, Y.; Qiu, Y. Advanced flexible skin-like pressure and strain sensors for human health monitoring. *Micromachines* **2021**, *12*, 695. [[CrossRef](#)]
35. Wang, J.; Dai, T.; Zhou, Y.; Mohamed, A.; Yuan, G.; Jia, H. Adhesive and high-sensitivity modified Ti₃C₂TX (MXene)-based organohydrogels with wide work temperature range for wearable sensors. *J. Colloid Interface Sci.* **2022**, *613*, 94–102. [[CrossRef](#)] [[PubMed](#)]
36. Jung, G.; Lee, H.; Park, H.; Kim, J.; Kim, J.W.; Kim, D.S.; Keum, K.; Lee, Y.H.; Ha, J.S. Temperature-tolerant flexible supercapacitor integrated with a strain sensor using an organohydrogel for wearable electronics. *Chem. Eng. J.* **2022**, *450*, 138379. [[CrossRef](#)]
37. Qin, Z.; Sun, X.; Zhang, H.; Yu, Q.; Wang, X.; He, S.; Yao, F.; Li, J. A transparent, ultrastretchable and fully recyclable gelatin organohydrogel based electronic sensor with broad operating temperature. *J. Mater. Chem. A* **2020**, *8*, 4447–4456. [[CrossRef](#)]
38. Yang, J.; Xu, Z.; Wang, J.; Gai, L.; Ji, X.; Jiang, H.; Liu, L. Antifreezing zwitterionic hydrogel electrolyte with high conductivity of 12.6 mS cm⁻¹ at -40° C through hydrated lithium ion hopping migration. *Adv. Funct. Mater.* **2021**, *31*, 2009438. [[CrossRef](#)]
39. Liu, Z.; Zhang, J.; Liu, J.; Long, Y.; Fang, L.; Wang, Q.; Liu, T. Highly compressible and superior low temperature tolerant supercapacitors based on dual chemically crosslinked PVA hydrogel electrolytes. *J. Mater. Chem. A* **2020**, *8*, 6219–6228. [[CrossRef](#)]

40. Yang, Y.; Wang, K.-P.; Zang, Q.; Shi, Q.; Wang, Y.; Xiao, Z.; Zhang, Q.; Wang, L. Anionic organo-hydrogel electrolyte with enhanced ionic conductivity and balanced mechanical properties for flexible supercapacitors. *J. Mater. Chem. A* **2022**, *10*, 11277–11287. [[CrossRef](#)]
41. Rong, Q.; Lei, W.; Huang, J.; Liu, M. Low temperature tolerant organohydrogel electrolytes for flexible solid-state supercapacitors. *Adv. Energy Mater.* **2018**, *8*, 1801967. [[CrossRef](#)]
42. Feng, E.; Li, J.; Zheng, G.; Yan, Z.; Li, X.; Gao, W.; Ma, X.; Yang, Z. Long-term anti-freezing active organohydrogel based superior flexible supercapacitor and strain sensor. *ACS Sustain. Chem. Eng.* **2021**, *9*, 7267–7276. [[CrossRef](#)]
43. Wang, P.; Wei, W.; Li, Z.; Duan, W.; Han, H.; Xie, Q. A superhydrophobic fluorinated PDMS composite as a wearable strain sensor with excellent mechanical robustness and liquid impalement resistance. *J. Mater. Chem. A* **2020**, *8*, 3509–3516. [[CrossRef](#)]
44. Huang, J.; Peng, S.; Gu, J.; Chen, G.; Gao, J.; Zhang, J.; Hou, L.; Yang, X.; Jiang, X.; Guan, L. Self-powered integrated system of a strain sensor and flexible all-solid-state supercapacitor by using a high performance ionic organohydrogel. *Mater. Horiz.* **2020**, *7*, 2085–2096. [[CrossRef](#)]
45. Ma, D.; Wu, X.; Wang, Y.; Liao, H.; Wan, P.; Zhang, L. Wearable, antifreezing, and healable epidermal sensor assembled from long-lasting moist conductive nanocomposite organohydrogel. *ACS Appl. Mater. Interfaces* **2019**, *11*, 41701–41709. [[CrossRef](#)] [[PubMed](#)]
46. Wang, X.; Wang, X.; Yin, J.; Li, N.; Zhang, Z.; Xu, Y.; Zhang, L.; Qin, Z.; Jiao, T. Mechanically robust, degradable and conductive MXene-composited gelatin organohydrogel with environmental stability and self-adhesiveness for multifunctional sensor. *Compos. Part B Eng.* **2022**, *241*, 110052. [[CrossRef](#)]
47. Yang, Z.; Huang, T.; Cao, P.; Cui, Y.; Nie, J.; Chen, T.; Yang, H.; Wang, F.; Sun, L. Carbonized silk nanofibers in biodegradable, flexible temperature sensors for extracellular environments. *ACS Appl. Mater. Interfaces* **2022**, *14*, 18110–18119. [[CrossRef](#)]
48. Lee, J.-H.; Chen, H.; Kim, E.; Zhang, H.; Wu, K.; Zhang, H.; Shen, X.; Zheng, Q.; Yang, J.; Jeon, S. Flexible temperature sensors made of aligned electrospun carbon nanofiber films with outstanding sensitivity and selectivity towards temperature. *Mater. Horiz.* **2021**, *8*, 1488–1498. [[CrossRef](#)] [[PubMed](#)]
49. Dai, Z.; Ding, S.; Lei, M.; Li, S.; Xu, Y.; Zhou, Y.; Zhou, B. A superhydrophobic and anti-corrosion strain sensor for robust underwater applications. *J. Mater. Chem. A* **2021**, *9*, 15282–15293. [[CrossRef](#)]
50. Hu, X.; Yang, F.; Wu, M.; Sui, Y.; Guo, D.; Li, M.; Kang, Z.; Sun, J.; Liu, J. A Super-Stretchable and Highly Sensitive Carbon Nanotube Capacitive Strain Sensor for Wearable Applications and Soft Robotics. *Adv. Mater. Technol.* **2022**, *7*, 2100769. [[CrossRef](#)]
51. Tsang, A.C.H.; Hui, K.N.; Hui, K.S.; Liu, B.; Yu, L.; Shi, B.; Huang, H. Ink-printed metal/graphene aerogel for glucose electro-oxidation. *Battery Energy* **2022**, *1*, 20220004. [[CrossRef](#)]
52. Shao, C.; Qiu, S.; Wu, G.; Cui, B.; Chu, H.; Zou, Y.; Xiang, C.; Xu, F.; Sun, L. Rambutan-like hierarchically porous carbon microsphere as electrode material for high-performance supercapacitors. *Carbon Energy* **2021**, *3*, 361–374. [[CrossRef](#)]
53. Zhang, Q.; Deng, C.; Huang, Z.; Zhang, Q.; Chai, X.; Yi, D.; Fang, Y.; Wu, M.; Wang, X.; Tang, Y. Dual-Silica Template-Mediated Synthesis of Nitrogen-Doped Mesoporous Carbon Nanotubes for Supercapacitor Applications. *Small* **2023**, *19*, 2205725. [[CrossRef](#)]
54. Wang, H.; Liu, C.; Li, B.; Liu, J.; Shen, Y.; Zhang, M.; Ji, K.; Mao, X.; Sun, R.; Zhou, F. Advances in Carbon-Based Resistance Strain Sensors. *ACS Appl. Electron. Mater.* **2023**, *5*, 674–689. [[CrossRef](#)]
55. Afroze, J.D.; Tong, L.; Abden, M.J.; Chen, Y. Multifunctional hierarchical graphene-carbon fiber hybrid aerogels for strain sensing and energy storage. *Adv. Compos. Hybrid Mater.* **2023**, *6*, 18. [[CrossRef](#)]
56. Bariya, M.; Nyein, H.Y.Y.; Javey, A. Wearable sweat sensors. *Nat. Electron.* **2018**, *1*, 160–171. [[CrossRef](#)]
57. Kim, S.; Xiao, X.; Chen, J. Advances in Photoplethysmography for Personalized Cardiovascular Monitoring. *Biosensors* **2022**, *12*, 863. [[CrossRef](#)] [[PubMed](#)]
58. Zhang, S.; Bick, M.; Xiao, X.; Chen, G.; Nashalian, A.; Chen, J. Leveraging triboelectric nanogenerators for bioengineering. *Matter* **2021**, *4*, 845–887. [[CrossRef](#)]
59. Zhou, Y.; Xiao, X.; Chen, G.; Zhao, X.; Chen, J. Self-powered sensing technologies for human Metaverse interfacing. *Joule* **2022**, *6*, 1381–1389. [[CrossRef](#)]
60. Rim, Y.S.; Bae, S.H.; Chen, H.; De Marco, N.; Yang, Y. Recent progress in materials and devices toward printable and flexible sensors. *Adv. Mater.* **2016**, *28*, 4415–4440. [[CrossRef](#)] [[PubMed](#)]
61. Araromi, O.A.; Graule, M.A.; Dorsey, K.L.; Castellanos, S.; Foster, J.R.; Hsu, W.-H.; Passy, A.E.; Vlassak, J.J.; Weaver, J.C.; Walsh, C.J. Ultra-sensitive and resilient compliant strain gauges for soft machines. *Nature* **2020**, *587*, 219–224. [[CrossRef](#)]
62. Chao, M.; Wang, Y.; Ma, D.; Wu, X.; Zhang, W.; Zhang, L.; Wan, P. Wearable MXene nanocomposites-based strain sensor with tile-like stacked hierarchical microstructure for broad-range ultrasensitive sensing. *Nano Energy* **2020**, *78*, 105187. [[CrossRef](#)]
63. Yi, J.; Xianyu, Y. Gold Nanomaterials-Implemented Wearable Sensors for Healthcare Applications. *Adv. Funct. Mater.* **2022**, *32*, 2113012. [[CrossRef](#)]
64. Peng, Z.; Shi, J.; Xiao, X.; Hong, Y.; Li, X.; Zhang, W.; Cheng, Y.; Wang, Z.; Li, W.J.; Chen, J. Self-charging electrostatic face masks leveraging triboelectrification for prolonged air filtration. *Nat. Commun.* **2022**, *13*, 7835. [[CrossRef](#)] [[PubMed](#)]
65. Yan, T.; Wu, Y.; Yi, W.; Pan, Z. Recent progress on fabrication of carbon nanotube-based flexible conductive networks for resistive-type strain sensors. *Sens. Actuators A Phys.* **2021**, *327*, 112755. [[CrossRef](#)]
66. He, S.; Hong, Y.; Liao, M.; Li, Y.; Qiu, L.; Peng, H. Flexible sensors based on assembled carbon nanotubes. *Aggregate* **2021**, *2*, e143. [[CrossRef](#)]

67. Wang, C.; Xia, K.; Wang, H.; Liang, X.; Yin, Z.; Zhang, Y. Advanced carbon for flexible and wearable electronics. *Adv. Mater.* **2019**, *31*, 1801072. [[CrossRef](#)]
68. Zhang, Y.; Xiao, Q.; Wang, Q.; Zhang, Y.; Wang, P.; Li, Y. A review of wearable carbon-based sensors for strain detection: Fabrication methods, properties, and mechanisms. *Text. Res. J.* **2023**, *93*, 2918–2940. [[CrossRef](#)]
69. Liu, F.; Xie, D.; Lv, F.; Shen, L.; Tian, Z.; Zhao, J. Additive Manufacturing of Stretchable Polyurethane/Graphene/Multiwalled Carbon Nanotube-Based Conducting Polymers for Strain Sensing. *ACS Appl. Nano Mater.* **2023**, *6*, 4522–4531. [[CrossRef](#)]
70. Chen, H.; Zhuo, F.; Zhou, J.; Liu, Y.; Zhang, J.; Dong, S.; Liu, X.; Elmarakbi, A.; Duan, H.; Fu, Y. Advances in graphene-based flexible and wearable strain sensors. *Chem. Eng. J.* **2023**, *464*, 142576. [[CrossRef](#)]
71. O'connell, M.J. *Carbon Nanotubes: Properties and Applications*; CRC Press: Boca Raton, FL, USA, 2018.
72. Maniecki, T.; Shtyka, O.; Mierczynski, P.; Ciesielski, R.; Czynkowska, A.; Leyko, J.; Mitukiewicz, G.; Dubkov, S.; Gromov, D. Carbon nanotubes: Properties, synthesis, and application. *Fibre Chem.* **2018**, *50*, 297–300. [[CrossRef](#)]
73. Popov, V.N. Carbon nanotubes: Properties and application. *Mater. Sci. Eng. R Rep.* **2004**, *43*, 61–102. [[CrossRef](#)]
74. Neto, A.C.; Guinea, F.; Peres, N.M.; Novoselov, K.S.; Geim, A.K. The electronic properties of graphene. *Rev. Mod. Phys.* **2009**, *81*, 109. [[CrossRef](#)]
75. Elapolu, M.S.; Tabarraei, A. Mechanical and fracture properties of polycrystalline graphene with hydrogenated grain boundaries. *J. Phys. Chem. C* **2021**, *125*, 11147–11158. [[CrossRef](#)]
76. Abergel, D.; Apalkov, V.; Berashevich, J.; Ziegler, K.; Chakraborty, T. Properties of graphene: A theoretical perspective. *Adv. Phys.* **2010**, *59*, 261–482. [[CrossRef](#)]
77. Kumar, S.; Nehra, M.; Kedia, D.; Dilbaghi, N.; Tankeshwar, K.; Kim, K.-H. Nanodiamonds: Emerging face of future nanotechnology. *Carbon* **2019**, *143*, 678–699. [[CrossRef](#)]
78. Mochalin, V.; Shenderova, O.; Ho, D.; Gogotsi, Y. The properties and applications of nanodiamonds. In *Nano-Enabled Medical Applications*; Jenny Stanford Publishing: New York, NY, USA, 2020; pp. 313–350.
79. Hilding, J.; Grulke, E.A.; George Zhang, Z.; Lockwood, F. Dispersion of carbon nanotubes in liquids. *J. Dispers. Sci. Technol.* **2003**, *24*, 1–41. [[CrossRef](#)]
80. Szroeder, P.; Sagaljanov, I.Y.; Radchenko, T.M.; Tatarenko, V.A.; Prylutsky, Y.I.; Strupiński, W. Effect of uniaxial stress on the electrochemical properties of graphene with point defects. *Appl. Surf. Sci.* **2018**, *442*, 185–188. [[CrossRef](#)]
81. Balog, R.; Jørgensen, B.; Nilsson, L.; Andersen, M.; Rienks, E.; Bianchi, M.; Fanetti, M.; Lægsgaard, E.; Baraldi, A.; Lizzit, S. Bandgap opening in graphene induced by patterned hydrogen adsorption. *Nat. Mater.* **2010**, *9*, 315–319. [[CrossRef](#)]
82. Zeiger, M.; Jäckel, N.; Mochalin, V.N.; Presser, V. Carbon onions for electrochemical energy storage. *J. Mater. Chem. A* **2016**, *4*, 3172–3196. [[CrossRef](#)]
83. Mohr, M.; Caron, A.; Herbeck-Engel, P.; Bennewitz, R.; Gluche, P.; Brühne, K.; Fecht, H.-J. Young's modulus, fracture strength, and Poisson's ratio of nanocrystalline diamond films. *J. Appl. Phys.* **2014**, *116*, 124308. [[CrossRef](#)]
84. Zhu, Y.; Murali, S.; Cai, W.; Li, X.; Suk, J.W.; Potts, J.R.; Ruoff, R.S. Graphene and graphene oxide: Synthesis, properties, and applications. *Adv. Mater.* **2010**, *22*, 3906–3924. [[CrossRef](#)]
85. Zhang, Y.; Lin, H.; Zhang, L.; Peng, S.; Weng, Z.; Wang, J.; Wu, L.; Zheng, L. Mechanical exfoliation assisted with carbon nanospheres to prepare a few-layer graphene for flexible strain sensor. *Appl. Surf. Sci.* **2023**, *611*, 155649. [[CrossRef](#)]
86. De Marchi, L.; Pretti, C.; Gabriel, B.; Marques, P.A.; Freitas, R.; Neto, V. An overview of graphene materials: Properties, applications and toxicity on aquatic environments. *Sci. Total Environ.* **2018**, *631*, 1440–1456. [[CrossRef](#)] [[PubMed](#)]
87. Turcheniuk, K.; Mochalin, V.N. Biomedical applications of nanodiamond. *Nanotechnology* **2017**, *28*, 252001. [[CrossRef](#)] [[PubMed](#)]
88. Petrák, V.; Živcová, Z.V.; Krýsová, H.; Frank, O.; Zukal, A.; Klimša, L.; Kopeček, J.; Taylor, A.; Kavan, L.; Mortet, V. Fabrication of porous boron-doped diamond on SiO₂ fiber templates. *Carbon* **2017**, *114*, 457–464. [[CrossRef](#)]
89. Wiora, N.; Mertens, M.; Mohr, M.; Bruehne, K.; Fecht, H.-J. Piezoresistivity of n-type conductive ultrananocrystalline diamond. *Diam. Relat. Mater.* **2016**, *70*, 145–150. [[CrossRef](#)]
90. Chauhan, S.; Jain, N.; Nagaich, U. Nanodiamonds with powerful ability for drug delivery and biomedical applications: Recent updates on in vivo study and patents. *J. Pharm. Anal.* **2020**, *10*, 1–12. [[CrossRef](#)]
91. Rifai, A.; Pirogova, E.; Fox, K. Diamond, carbon nanotubes and graphene for biomedical applications. In *Reference Module in Biomedical Sciences*; Elsevier: Amsterdam, The Netherlands, 2018; pp. 1–11.
92. Sun, H.; Bu, Y.; Liu, H.; Wang, J.; Yang, W.; Li, Q.; Guo, Z.; Liu, C.; Shen, C. Superhydrophobic conductive rubber band with synergistic dual conductive layer for wide-range sensitive strain sensor. *Sci. Bull.* **2022**, *67*, 1669–1678. [[CrossRef](#)]
93. Ahuja, P.; Akiyama, S.; Ujjain, S.K.; Kukobat, R.; Vallejos-Burgos, F.; Futamura, R.; Hayashi, T.; Kimura, M.; Tomanek, D.; Kaneko, K. A water-resilient carbon nanotube based strain sensor for monitoring structural integrity. *J. Mater. Chem. A* **2019**, *7*, 19996–20005. [[CrossRef](#)]
94. Huang, J.; Li, J.; Xu, X.; Hua, L.; Lu, Z. In situ loading of polypyrrole onto aramid nanofiber and carbon nanotube aerogel fibers as physiology and motion sensors. *ACS Nano* **2022**, *16*, 8161–8171. [[CrossRef](#)]
95. Badatya, S.; Bharti, D.K.; Sathish, N.; Srivastava, A.K.; Gupta, M.K. Humidity sustainable hydrophobic poly(vinylidene fluoride)-carbon nanotubes foam based piezoelectric nanogenerator. *ACS Appl. Mater. Interfaces* **2021**, *13*, 27245–27254. [[CrossRef](#)] [[PubMed](#)]

96. Li, H.; Yang, Y.; Li, M.; Zhu, Y.; Zhang, C.; Zhang, R.; Song, Y. Frost-resistant and ultrasensitive strain sensor based on a tannic acid-nanocellulose/sulfonated carbon nanotube-reinforced polyvinyl alcohol hydrogel. *Int. J. Biol. Macromol.* **2022**, *219*, 199–212. [[CrossRef](#)] [[PubMed](#)]
97. Zhang, C.; Song, S.; Li, Q.; Wang, J.; Liu, Z.; Zhang, S.; Zhang, Y. One-pot facile fabrication of covalently cross-linked carbon nanotube/PDMS composite foam as a pressure/temperature sensor with high sensitivity and stability. *J. Mater. Chem. C* **2021**, *9*, 15337–15345. [[CrossRef](#)]
98. Gao, J.; Wu, L.; Guo, Z.; Li, J.; Xu, C.; Xue, H. A hierarchical carbon nanotube/SiO₂ nanoparticle network induced superhydrophobic and conductive coating for wearable strain sensors with superior sensitivity and ultra-low detection limit. *J. Mater. Chem. C* **2019**, *7*, 4199–4209. [[CrossRef](#)]
99. Zhu, W.-B.; Xue, S.-S.; Zhang, H.; Wang, Y.-Y.; Huang, P.; Tang, Z.-H.; Li, Y.-Q.; Fu, S.-Y. Direct ink writing of a graphene/CNT/silicone composite strain sensor with a near-zero temperature coefficient of resistance. *J. Mater. Chem. C* **2022**, *10*, 8226–8233. [[CrossRef](#)]
100. Lee, H.; Jung, G.; Keum, K.; Kim, J.W.; Jeong, H.; Lee, Y.H.; Kim, D.S.; Ha, J.S. A textile-based temperature-tolerant stretchable supercapacitor for wearable electronics. *Adv. Funct. Mater.* **2021**, *31*, 2106491. [[CrossRef](#)]
101. Singh, K.; Gupta, M.; Tripathi, C. Fabrication of flexible and sensitive laser-patterned serpentine-structured graphene–CNT paper for strain sensor applications. *Appl. Phys. A* **2022**, *128*, 1131. [[CrossRef](#)]
102. Lu, D.; Liao, S.; Chu, Y.; Cai, Y.; Wei, Q.; Chen, K.; Wang, Q. Highly durable and fast response fabric strain sensor for movement monitoring under extreme conditions. *Adv. Fiber Mater.* **2023**, *5*, 223–234. [[CrossRef](#)]
103. Kulha, P.; Kromka, A.; Babchenko, O.; Vanecek, M.; Husak, M.; Williams, O.A.; Haenen, K. Nanocrystalline diamond piezoresistive sensor. *Vacuum* **2009**, *84*, 53–56. [[CrossRef](#)]
104. Rehman, A.; Houshyar, S.; Reineck, P.; Padhye, R.; Wang, X. Multifunctional smart fabrics through nanodiamond-polyaniline nanocomposites. *ACS Appl. Polym. Mater.* **2020**, *2*, 4848–4855. [[CrossRef](#)]
105. Bähr, M.; Käpplinger, I.; Pobedinskas, P.; Frank, T.; Grün, A.; Haenen, K.; Ortlepp, T. Pressure Sensor Devices Featuring a Chemical Passivation Made of a Locally Synthesized Diamond Layer. *Phys. Status Solidi (a)* **2023**, *220*, 2200309. [[CrossRef](#)]
106. Yu, X.; Chen, X.; Ding, X.; Yu, X.; Zhao, X.; Chen, X. Facile fabrication of flower-like MoS₂/nanodiamond nanocomposite toward high-performance humidity detection. *Sens. Actuators B Chem.* **2020**, *317*, 128168. [[CrossRef](#)]
107. Ding, Y.-R.; Xue, C.-H.; Fan, Q.-Q.; Zhao, L.-L.; Tian, Q.-Q.; Guo, X.-J.; Zhang, J.; Jia, S.-T.; An, Q.-F. Fabrication of superhydrophobic conductive film at air/water interface for flexible and wearable sensors. *Chem. Eng. J.* **2021**, *404*, 126489. [[CrossRef](#)]
108. Zhu, S.; Lu, Y.; Wang, S.; Sun, H.; Yue, Y.; Xu, X.; Mei, C.; Xiao, H.; Fu, Q.; Han, J. Interface design of stretchable and environment-tolerant strain sensors with hierarchical nanocellulose-supported graphene nanocomplexes. *Compos. Part A Appl. Sci. Manuf.* **2023**, *164*, 107313. [[CrossRef](#)]
109. Ma, S.; Jia, T.; Wang, C.; Xu, H.; Zhou, H.; Zhao, X.; Chen, C.; Wang, D.; Liu, C.; Qu, C. Anisotropic MWCNT/polyimide aerogels with multifunctional EMI shielding and strain sensing capabilities. *Compos. Part A Appl. Sci. Manuf.* **2022**, *163*, 107208. [[CrossRef](#)]
110. Barlian, A.A.; Park, W.-T.; Mallon, J.R.; Rastegar, A.J.; Pruitt, B.L. Semiconductor piezoresistance for microsystems. *Proc. IEEE* **2009**, *97*, 513–552. [[CrossRef](#)] [[PubMed](#)]
111. Zhai, J.; Zhang, Y.; Cui, C.; Li, A.; Wang, W.; Guo, R.; Qin, W.; Ren, E.; Xiao, H.; Zhou, M. Flexible waterborne polyurethane/cellulose nanocrystal composite aerogels by integrating graphene and carbon nanotubes for a highly sensitive pressure sensor. *ACS Sustain. Chem. Eng.* **2021**, *9*, 14029–14039. [[CrossRef](#)]
112. Deng, Y.; Wang, H.; Zhang, K.; Shao, J.; Qiu, J.; Wu, J.; Wu, Y.; Yan, L. A high-voltage quasi-solid-state flexible supercapacitor with a wide operational temperature range based on a low-cost “water-in-salt” hydrogel electrolyte. *Nanoscale* **2021**, *13*, 3010–3018. [[CrossRef](#)]
113. Chen, X.; Liu, H.; Zheng, Y.; Zhai, Y.; Liu, X.; Liu, C.; Mi, L.; Guo, Z.; Shen, C. Highly compressible and robust polyimide/carbon nanotube composite aerogel for high-performance wearable pressure sensor. *ACS Appl. Mater. Interfaces* **2019**, *11*, 42594–42606. [[CrossRef](#)]
114. Sun, H.; Zhao, Y.; Jiao, S.; Wang, C.; Jia, Y.; Dai, K.; Zheng, G.; Liu, C.; Wan, P.; Shen, C. Environment tolerant conductive nanocomposite organohydrogels as flexible strain sensors and power sources for sustainable electronics. *Adv. Funct. Mater.* **2021**, *31*, 2101696. [[CrossRef](#)]
115. Zang, X.; Zhang, R.; Zhen, Z.; Lai, W.; Yang, C.; Kang, F.; Zhu, H. Flexible, temperature-tolerant supercapacitor based on hybrid carbon film electrodes. *Nano Energy* **2017**, *40*, 224–232. [[CrossRef](#)]
116. Nankali, M.; Nouri, N.M.; Navidbakhsh, M.; Malek, N.G.; Amindehghan, M.A.; Shahtoori, A.M.; Karimi, M.; Amjadi, M. Highly stretchable and sensitive strain sensors based on carbon nanotube–elastomer nanocomposites: The effect of environmental factors on strain sensing performance. *J. Mater. Chem. C* **2020**, *8*, 6185–6195. [[CrossRef](#)]
117. Hou, X.; Zhang, Q.; Wang, L.; Gao, G.; Lu, W. Low-temperature-resistant flexible solid supercapacitors based on organohydrogel electrolytes and microvoid-incorporated reduced graphene oxide electrodes. *ACS Appl. Mater. Interfaces* **2021**, *13*, 12432–12441. [[CrossRef](#)]
118. Xu, X.; Chen, Y.; He, P.; Wang, S.; Ling, K.; Liu, L.; Lei, P.; Huang, X.; Zhao, H.; Cao, J. Wearable CNT/Ti₃C₂T_x MXene/PDMS composite strain sensor with enhanced stability for real-time human healthcare monitoring. *Nano Res.* **2021**, *14*, 2875–2883. [[CrossRef](#)]

119. Zhu, S.; Peng, S.; Qiang, Z.; Ye, C.; Zhu, M. Cryogenic-environment resistant, highly elastic hybrid carbon foams for pressure sensing and electromagnetic interference shielding. *Carbon* **2022**, *193*, 258–271. [[CrossRef](#)]
120. Zhang, J.; Liu, X.; Feng, H.; Wang, C.; Rong, Q.; Liu, M. Conductive, sensing stable and mechanical robust silicone rubber composites for large-strain sensors. *Polym. Compos.* **2021**, *42*, 6394–6402. [[CrossRef](#)]
121. Sadi, M.S.; Kumpikaitė, E. Highly conductive composites using polypyrrole and carbon nanotubes on polydopamine functionalized cotton fabric for wearable sensing and heating applications. *Cellulose* **2023**, *30*, 7981–7999. [[CrossRef](#)]
122. Zhang, J.; Liu, J.; Zhao, Z.; Sun, W.; Zhao, G.; Liu, J.; Xu, J.; Li, Y.; Liu, Z.; Li, Y. Calotropis gigantea Fiber-Based Sensitivity-Tunable Strain Sensors with Insensitive Response to Wearable Microclimate Changes. *Adv. Fiber Mater.* **2023**, *5*, 1378–1391. [[CrossRef](#)]
123. Jiao, E.; Wu, K.; Liu, Y.; Zhang, H.; Zheng, H.; Xu, C.-a.; Shi, J.; Lu, M. Nacre-like robust cellulose nanofibers/MXene films with high thermal conductivity and improved electrical insulation by nanodiamond. *J. Mater. Sci.* **2022**, *57*, 2584–2596. [[CrossRef](#)]
124. Wang, X.; Cao, W.; Su, Z.; Zhao, K.; Dai, B.; Gao, G.; Zhao, J.; Zhao, K.; Wang, Z.; Sun, T. Fabrication of High Thermal Conductivity Nanodiamond/Aramid Nanofiber Composite Films with Superior Multifunctional Properties. *ACS Appl. Mater. Interfaces* **2023**, *15*, 27130–27143. [[CrossRef](#)]
125. Li, L.; Bai, Y.; Li, L.; Wang, S.; Zhang, T. A superhydrophobic smart coating for flexible and wearable sensing electronics. *Adv. Mater.* **2017**, *29*, 1702517. [[CrossRef](#)]
126. Wang, L.; Chen, Y.; Lin, L.; Wang, H.; Huang, X.; Xue, H.; Gao, J. Highly stretchable, anti-corrosive and wearable strain sensors based on the PDMS/CNTs decorated elastomer nanofiber composite. *Chem. Eng. J.* **2019**, *362*, 89–98. [[CrossRef](#)]
127. Liu, H.; Xu, T.; Cai, C.; Liu, K.; Liu, W.; Zhang, M.; Du, H.; Si, C.; Zhang, K. Multifunctional superelastic, superhydrophilic, and ultralight nanocellulose-based composite carbon aerogels for compressive supercapacitor and strain sensor. *Adv. Funct. Mater.* **2022**, *32*, 2113082. [[CrossRef](#)]
128. Chen, Y.; Wang, L.; Wu, Z.; Luo, J.; Li, B.; Huang, X.; Xue, H.; Gao, J. Super-hydrophobic, durable and cost-effective carbon black/rubber composites for high performance strain sensors. *Compos. Part B Eng.* **2019**, *176*, 107358. [[CrossRef](#)]
129. Seyedin, S.; Zhang, P.; Naebe, M.; Qin, S.; Chen, J.; Wang, X.; Razal, J.M. Textile strain sensors: A review of the fabrication technologies, performance evaluation and applications. *Mater. Horiz.* **2019**, *6*, 219–249. [[CrossRef](#)]
130. Qu, R.; Zhang, W.; Liu, N.; Zhang, Q.; Liu, Y.; Li, X.; Wei, Y.; Feng, L. Antioil Ag₃PO₄ nanoparticle/polydopamine/Al₂O₃ sandwich structure for complex wastewater treatment: Dynamic catalysis under natural light. *ACS Sustain. Chem. Eng.* **2018**, *6*, 8019–8028. [[CrossRef](#)]
131. Wu, H.; Liu, Q.; Du, W.; Li, C.; Shi, G. Transparent polymeric strain sensors for monitoring vital signs and beyond. *ACS Appl. Mater. Interfaces* **2018**, *10*, 3895–3901. [[CrossRef](#)] [[PubMed](#)]
132. Liu, X.; Lu, C.; Wu, X.; Zhang, X. Self-healing strain sensors based on nanostructured supramolecular conductive elastomers. *J. Mater. Chem. A* **2017**, *5*, 9824–9832. [[CrossRef](#)]
133. Pang, Y.; Yang, Z.; Han, X.; Jian, J.; Li, Y.; Wang, X.; Qiao, Y.; Yang, Y.; Ren, T.-L. Multifunctional mechanical sensors for versatile physiological signal detection. *ACS Appl. Mater. Interfaces* **2018**, *10*, 44173–44182. [[CrossRef](#)]
134. Houshyar, S.; Nayak, R.; Padhye, R.; Shanks, R.A. Fabrication and characterization of nanodiamond coated cotton fabric for improved functionality. *Cellulose* **2019**, *26*, 5797–5806. [[CrossRef](#)]
135. Houshyar, S.; Padhye, R.; Shanks, R.A.; Nayak, R. Nanodiamond fabrication of superhydrophilic wool fabrics. *Langmuir* **2019**, *35*, 7105–7111. [[CrossRef](#)] [[PubMed](#)]

Disclaimer/Publisher’s Note: The statements, opinions and data contained in all publications are solely those of the individual author(s) and contributor(s) and not of MDPI and/or the editor(s). MDPI and/or the editor(s) disclaim responsibility for any injury to people or property resulting from any ideas, methods, instructions or products referred to in the content.